Lecture 4. Measurements without contact in heat transfer : radiation thermometry

Part A: principles, implementation and pitfalls

J.-C. Krapez[1]

[1] ONERA, The French Aerospace Lab, Salon de Provence, France

E-mail: krapez@onera.fr

Abstract. The objective of this lecture is to present the main features of spectral and multispectral radiometry when applied for the purpose of temperature measurement, in particular pyrometry. The amount of thermal radiation emitted by a surface is only a fraction of the radiation emitted by a blackbody at the same temperature. The corresponding ratio is called emissivity. It is an additional unknown parameter which depends on material, wavelength, direction, and surface state. In passive radiation thermometry, whatever the number of considered wavelengths, we face an underdetermined problem, notwithstanding the fact that the atmosphere between the sensed surface and the sensor introduces itself additional unknown parameters. A series of solutions have been presented to solve the problem of emissivity and temperature separation in the field of multiwavelength pyrometry. Their performance and inherent difficulties will be discussed.

List of acronyms:

- **LSMWP** Least-Squares Multi-Wavelength Pyrometry
- **MCMC** Markov Chain Monte Carlo
- **MLE** Maximum Likelihood Estimation
- **MWP** Multi-Wavelength Pyrometry
- **OLS** Ordinary Least Squares
- **RMS** Root Mean Squares
- **TES** Temperature Emissivity Separation

Scope

1. Introduction

Matter spontaneously emits electromagnetic radiation in a broad spectrum encompassing UV, visible light, infrared (IR) and microwaves. The radiance emitted by a surface depends on wavelength, temperature, direction and on the considered matter. For a solid material it also depends on the surface state, e.g. roughness and possibly the presence of corrosion.
Obviously, because the emitted radiance is quite sensitive to temperature, the measurement of the emitted power at a given wavelength could be used to infer the temperature. This idea is at the origin of pyrometry, thermography, and microwave radiometry.
However, the spectral radiance emitted by a material not only depends on the temperature but also on its spectral emissivity, which has thus to be known or evaluated in the same time as the temperature. On the other hand, before reaching a remote optical sensor, the emitted radiation has been attenuated by the atmosphere. In addition it has been combined with the radiation emitted by the atmosphere itself and the environmental radiation reflected by the aimed surface.
Evaluating the temperature from the at-sensor radiance is thus not an easy task. In this paper we will present some methods that enable estimating the surface temperature. A particular emphasis will be given to the temperature-emissivity separation problem.

2. Basic relations for the measured thermal radiance

2.1. Blackbody radiance

The maximum radiance emitted at given wavelength and temperature is described by the Planck's law (blackbody radiance) [1]:

$$B(\lambda,T)=\frac{C_1}{\lambda^5}\left[\exp\left(\frac{C_2}{\lambda T}\right)-1\right]^{-1} \tag{1}$$

The blackbody radiance $B(\lambda,T)$ is expressed in W/m^3/sr, wavelength λ is in m, temperature T in K, with the constants C_1 = 1.191·10^{-16} W·m^2 and C_2 = 1.439·10^{-2} m·K (notice that the blackbody radiance does not depend on direction). The blackbody radiance as expressed by the Planck's law, is described versus wavelength in figure 1 for different temperature values (curves with a continuous line). The maximum emission is observed at a particular wavelength $\lambda_{\max}$ such that $\exp(x_{\max})(5-x_{\max})=5$ where $x_{\max}\equiv C_2/\lambda_{\max}T$. The solution is $x_{\max}\approx 4.965$ which corresponds to $\lambda_{\max}T\approx 2898\,\mu mK$ (Wien's displacement law). Hence, the peak emissive intensity shifts to shorter wavelengths as temperature rises, in inverse proportion to T.

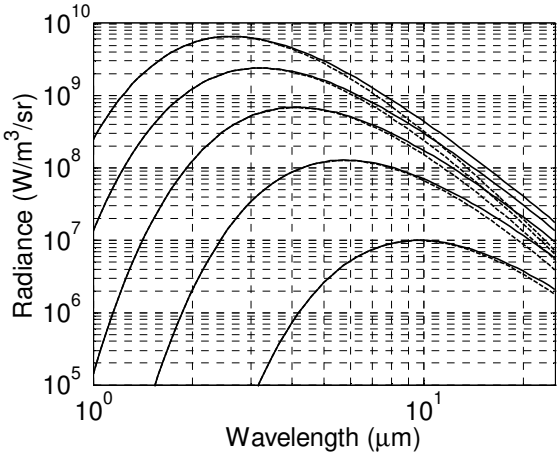

Figure 1. Blackbody radiance vs. wavelength for T=300K, 500K, 700K, 900K and 1100K (from bottom to top). Planck's law : continuous lines, Wien's law : dashed lines.

A common approximation to the Plank's law is the Wien's law which has been plotted in figure 1 as well (in dashed lines):

$$B_W(\lambda,T)=\frac{C_1}{\lambda^5}\exp\left(-\frac{C_2}{\lambda T}\right) \tag{2}$$

When using the Wien's law, the approximation error increases with wavelength, yet, the Wien's law can be consider quite accurate in the rising part of the radiance curve. As a matter of fact, at the apex of the curve, the error has reaches 0.7% only. Also, it is less than 1% as long as the product λT is lower than $3124\ \mu mK$.

The sensitivity of the blackbody radiance to the temperature, when considering the Planck's law, is plotted in figure 2. Figure 2-left refers to the absolute sensitivity $S=\partial B/\partial T$ whereas figure 2-right refers to the relative sensitivity $B^{-1}\partial B/\partial T$. The maximum of the absolute sensitivity is observed at a wavelength $\lambda_{S\max}$ such that $\exp(x_{S\max})(6-x_{S\max})=6+x_{S\max}$ where $x_{S\max}\equiv C_2/\lambda_{S\max}T$. The solution is $x_{S\max}\approx 5.969$ which corresponds to $\lambda_{S\max}T=2410\ \mu mK$. Notice that for a blackbody at 300K, the maximum of radiance is observed at the wavelength $\lambda_{\max}=9.65\ \mu m$ (see figure 1); however the maximum sensitivity to temperature variations is observed at a shorter wavelength, namely at $\lambda_{S\max}=8.03\ \mu m$ (see figure 2-left). On the other hand, the *relative* sensitivity is continuously decreasing (see figure 2-right). The asymptotic evolution is actually like $1/\lambda$ at short wavelengths. The decreasing nature of the relative sensitivity would thus favour short wavelengths for temperature measurement. However, in the meantime, the radiance progressively decreases at short wavelengths (see figure 1). Actually, several parameters should be considered when selecting a radiative sensor together with a spectral range for temperature measurement. One should evaluate the expected radiance in the temperature range of interest, its absolute and/or relative sensitivity,

together with the spectral detectivity of the candidate sensors or the corresponding noise (see e.g. [2]).

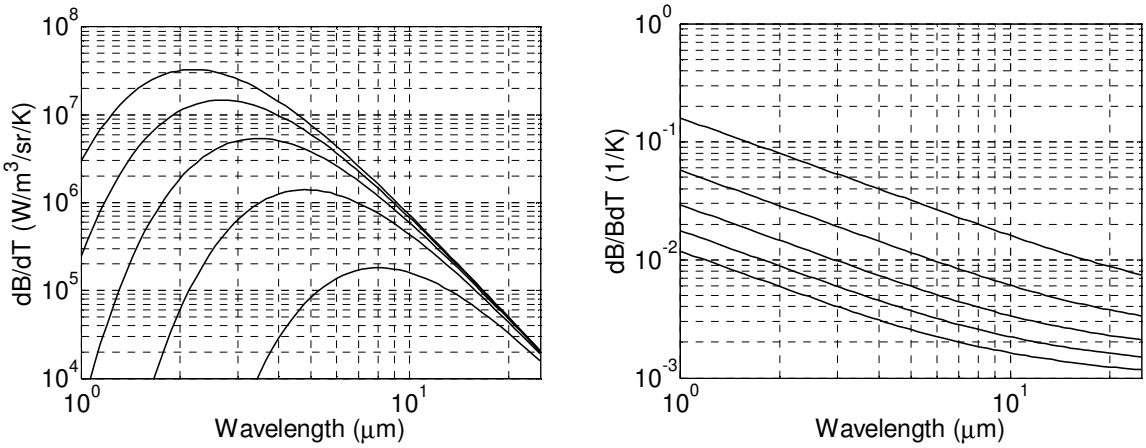

Figure 2. Absolute (left) and relative (right) sensitivity of the blackbody radiance to temperature for T=300K, 500K, 700K, 900K and 1100K (resp. from bottom to top and top to bottom).

2.2. Emissivity and related radiative parameters

Consider a surface at temperature T and a direction defined by the zenith and azimuthal angles (θ,φ). The ratio between the radiance effectively emitted by the surface in this direction at wavelength λ, namely $L(\lambda,T,\theta,\varphi)$, and the blackbody radiance $B_P(\lambda,T)$ at same wavelength and same temperature, is called *emissivity*:

$$\varepsilon = L(\lambda,T,\theta,\varphi)/B(\lambda,T); \quad \varepsilon \le 1 \tag{3}$$

Since the emissivity generally depends on wavelength and direction and since it may also depend on the surface temperature, we will write it as $\varepsilon = \varepsilon(\lambda,T,\theta,\varphi)$. However, if the temperature of interest is quite narrow, we may drop the T dependency for convenience and consider only $\varepsilon = \varepsilon(\lambda,\theta,\varphi)$.

From the analysis of the radiation in an enclosure we can state the following relation between the emissivity and the hemispherical directional reflectance (assuming isotropic incoming radiance) [1]:

$$\varepsilon(\lambda,\theta,\varphi) + \rho^{\cap'}(\lambda,\theta,\varphi) = 1 \tag{4}$$

Also, the energy conservation law for an opaque material tells that the energy that is not absorbed by the surface is reflected in all directions. It leads to the following relation between the absorptivity and the directional hemispherical reflectance:

$$\alpha(\lambda,\theta,\varphi) + \rho^{'\cap}(\lambda,\theta,\varphi) = 1 \tag{5}$$

On the other side the Helmholtz reciprocity principle leads to (for isotropic incoming radiance):

$$\rho^{\cap'}(\lambda,\theta,\varphi)=\rho'^{\cap}(\lambda,\theta,\varphi) \tag{6}$$

which, from eq. (4) and (5), leads itself to the second Kirchhoff's law which states that the spectral emissivity in a given direction (θ,φ) is equal to the spectral absorptivity in the same direction:

$$\varepsilon(\lambda,\theta,\varphi)=\alpha(\lambda,\theta,\varphi) \tag{7}$$

2.3. Expression of the measured radiance

Assume now that an optical sensor is in the direction (θ,φ) to perform a measurement of the surface temperature. The radiance of the radiation leaving the surface in this direction, namely $L(\lambda,T,\theta,\varphi)$, is the sum of the radiance emitted by the surface and the contribution of the radiation of radiance $L^{\downarrow}(\lambda,\theta_i,\varphi_i)$ coming from the environment in all incident directions (θ_i,φ_i) of the upper hemisphere and then reflected by the surface (in this course, without loss of generality, we will generally consider that the surface is facing up):

$$L(\lambda,T,\theta,\varphi)=\varepsilon(\lambda,\theta,\varphi)B(\lambda,T)+\int_{2\pi}\rho''(\lambda,\theta,\varphi,\theta_i,\varphi_i)L^{\downarrow}(\lambda,\theta_i,\varphi_i)\cos\theta_i d\Omega_i \tag{8}$$

where $\rho''(\lambda,\theta,\varphi,\theta_i,\varphi_i)$ is the bidirectional reflectance.
The radiance received by the optical detector, which will be called $L_s(\lambda,T,\theta,\varphi)$, encompasses both the radiance leaving the aimed surface and attenuated along the optical path, namely $\tau(\lambda,\theta,\varphi)L(\lambda,T,\theta,\varphi)$, where $\tau(\lambda,\theta,\varphi)$ is the transmission coefficient through the air, and the radiance $L^{\uparrow}(\lambda,\theta,\varphi)$ which is self-emitted by the atmosphere along this path:

$$L_s(\lambda,T,\theta,\varphi)=\tau(\lambda,\theta,\varphi)L(\lambda,T,\theta,\varphi)+L^{\uparrow}(\lambda,\theta,\varphi) \tag{9}$$

The general radiation thermometry equation is finally:

$$L_s(\lambda,T,\theta,\varphi)=\tau(\lambda,\theta,\varphi)\left[\begin{array}{l}\varepsilon(\lambda,\theta,\varphi)B(\lambda,T)\\+\int_{2\pi}\rho''(\lambda,\theta,\varphi,\theta_i,\varphi_i)L^{\downarrow}(\lambda,\theta_i,\varphi_i)\cos\theta_i d\Omega_i\end{array}\right]+L^{\uparrow}(\lambda,\theta,\varphi) \tag{10}$$

The optical sensor integrates the radiance over a narrow spectral band of width $\Delta\lambda$ centred at the wavelength λ. It delivers an electrical signal and, thanks to a calibration performed with a blackbody brought close to the sensor, a relationship can be established between this signal and the radiance $L_s(\lambda,T,\theta,\varphi)$ integrated over the spectral band of width $\Delta\lambda$. Since the

bandwidth $\Delta\lambda$ is small, the relationship is directly with the radiance at the wavelength λ, namely $L_s(\lambda,T,\theta,\varphi)$. After proper scaling of the signal S_λ we can consider that it is a clear representation of the incoming radiance $L_s(\lambda,T,\theta,\varphi)$, except it is affected by an experimental noise e_λ that for now we will consider simply to be additive:

$$S_\lambda = L_s(\lambda,T,\theta,\varphi) + e_\lambda \tag{11}$$

Notice that the calibration and the scaling should incorporate the contributions of the sensor optics (transmission and self-emission). Care should thus be taken that these contributions don't change between the time interval separating the calibration process and the temperature measurements themselves.

2.4. Simplification of the radiative equation

The objective is to evaluate the surface temperature from the measurement of the radiance $L_s(\lambda,T,\theta,\varphi)$ through the recording of the signal S_λ (see eq. (11)). At this point we have to deal with several unknowns: the transmission coefficient $\tau(\lambda,\theta,\varphi)$ and the self-emission of the atmosphere $L^{\uparrow}(\lambda,\theta,\varphi)$ along the line of sight, the hemispherical environmental radiance $L^{\downarrow}(\lambda,\theta_i,\varphi_i)$, the bidirectional reflectance $\rho''(\lambda,\theta,\varphi,\theta_i,\varphi_i)$ for all incident directions (θ_i,φ_i) and the directional emissivity $\varepsilon(\lambda,\theta,\varphi)$. Only when all these parameters are determined can we expect evaluating the blackbody radiance $B(\lambda,T)$ and then inferring the temperature.
A common approximation is to consider that the surface is Lambertian, i.e. its optical properties are direction-independent. Equation (10) is then simplified as follows:

$$L(\lambda,T) = \varepsilon(\lambda)B(\lambda,T) + (1-\varepsilon(\lambda))L^{\downarrow}(\lambda) \tag{12}$$

where $L^{\downarrow}(\lambda,T)$ is the mean environmental radiance (i.e. equivalent isotropic radiance) defined according to:

$$L^{\downarrow}(\lambda,T) = \frac{1}{\pi}\int_{2\pi} L^{\downarrow}(\lambda,\theta_i,\varphi_i)\cos\theta_i d\Omega_i \tag{13}$$

We then have access to the at-sensor spectral radiance:

$$L_s(\lambda,T,\theta,\varphi) = \tau(\lambda,\theta,\varphi)\left[\varepsilon(\lambda)B(\lambda,T) + (1-\varepsilon(\lambda))L^{\downarrow}(\lambda)\right] + L^{\uparrow}(\lambda,\theta,\varphi) \tag{14}$$

Generally speaking, when dealing with temperature measurement based on thermal radiation, we face two problems:

- first we have to correct the influence of the environment (reflections from nearby surfaces and from the atmosphere, along-the-path self-emission of the atmosphere and along-the-path attenuation);
- then we have to *separate emissivity and temperature*.

The atmosphere contribution through attenuation and self-emission is particularly relevant when the measurement is performed from large distances, as for example in airborne and satellite remote sensing. Specific methods for atmosphere correction have been developed for these applications. Emissivity and temperature separation methods that take advantage of the presence of the atmosphere where devised and we refer the reader to [3] for a review.
For the remaining of this presentation we will assume that an atmosphere correction has already been applied. This means, in the case of remote sensing applications, that the upwelling radiance $L^{\uparrow}(\lambda,\theta,\varphi)$, the transmission coefficient $\tau(\lambda,\theta,\varphi)$ and the downwelling mean radiance $L^{\downarrow}(\lambda)$ have been evaluated through simulations with a computer program designed to model atmospheric propagation of electromagnetic radiation like MODTRAN [4] or MATISSE [5].

Upon subtracting $L^{\uparrow}(\lambda,\theta,\varphi)$ from the signal and then dividing by $\tau(\lambda,\theta,\varphi)$ we obtain a transformed signal that is a representation of the surface-leaving radiance $L(\lambda,T,\theta,\varphi)$ as expressed in eq. (8):

$$\begin{aligned} S_\lambda &= L(\lambda,T,\theta,\varphi)+e_\lambda \\ &= \varepsilon(\lambda,\theta,\varphi)B(\lambda,T)+\int_{2\pi}\rho^{''}(\lambda,\theta,\varphi,\theta_i,\varphi_i)L^{\downarrow}(\lambda,\theta_i,\varphi_i)\cos\theta_i d\Omega_i+e_\lambda \end{aligned} \tag{15}$$

where, although having been transformed, the same notations have been kept for the new signal S_λ and the corresponding noise e_λ.
In the case of Lambertian surfaces the new signal access to the surface-leaving radiance $L(\lambda,T)$ as expressed in eq. (12):

$$\begin{aligned} S_\lambda &= L(\lambda,T)+e_\lambda \\ &= \varepsilon(\lambda)B(\lambda,T)+(1-\varepsilon(\lambda))L^{\downarrow}(\lambda)+e_\lambda \end{aligned} \tag{16}$$

Notice that eq. (16) can be modified into:

$$\begin{aligned} S_\lambda &= L(\lambda,T)+e_\lambda \\ &= \varepsilon(\lambda)\left(B(\lambda,T)-L^{\downarrow}(\lambda)\right)+L^{\downarrow}(\lambda)+e_\lambda \end{aligned} \tag{17}$$

2.5. Reflection component

There are different approaches for dealing with the reflection contribution, namely $\int_{2\pi} \rho^{''}(\lambda,\theta,\varphi,\theta_i,\varphi_i) L^{\downarrow}(\lambda,\theta_i,\varphi_i)\cos\theta_i d\Omega_i$ in the general case or $(1-\varepsilon(\lambda))L^{\downarrow}(\lambda)$ for lambertian surfaces.
In the case of small-scale laboratory experiments, *active pyrometry* with an additional heat source provides an efficient means for getting rid of the reflection term. Photothermal pyrometry is an example where an additional radiative heat source is provided for the purpose of slightly heating the test material dynamically [4]-[9]. The source is either pulsed or modulated. Usually, the heat source is a laser beam aimed at the region of interest. A pyrometer is then used to measure the slight variations of the radiance (in a spectral band not including the wavelength of the radiative heat source). By considering only the variations of radiance, not the initial or DC level (as easily obtained in the modulated regime by applying lock-in detection), the contribution of the spurious reflections is eliminated since those are constant in time. Only remains a signal proportional to $\varepsilon(\lambda)\partial B/\partial T(\lambda,T)$. Furthermore, by implementing two-color pyrometry at two wavelengths λ_1 and λ_2, we can get rid of the emissivity influence (in the same way as in the static regime, as described later in § 4), and obtain a signal that depends on both $\partial B/\partial T(\lambda_1,T)$ and $\partial B/\partial T(\lambda_2,T)$ from which temperature is then easily inferred.

In remote sensing, since the downwelling mean radiance $L^{\downarrow}(\lambda)$ have already been computed with an atmospheric propagation model (in the same time as the upwelling radiance $L^{\uparrow}(\lambda,\theta,\varphi)$ and the transmission coefficient $\tau(\lambda,\theta,\varphi)$), the obtained value will be substituted in eq. (17). The remaining unknown parameters are then the emissivity $\varepsilon(\lambda)$ and the temperature T appearing in the blackbody radiance $B(\lambda,T)$.

2.6. Introduction to the problem of temperature-emissivity separation

Whatever the configuration: active (see §2.5) or passive (see eq. (15), (16) or (17)), radiative thermometry faces an ambiguity problem knowing that a decrease or an increase of the emissivity can be fully compensated by an increase, resp. a decrease in temperature. Whatever the measurement wavelength, the observed signal may be explained by an infinite number of couples of emissivity values and temperature values.

It is then clear that an evaluation of the emissivity is necessary to infer the temperature from the measurement of the emitted radiance. An indirect approach consists in measuring the directional hemispherical reflectance and using equation (4), (5) and (6) to infer the directional emissivity. This requires using an additional radiation source and bringing close to the characterized surface an integrating hemisphere to collect all the reflected radiation. This

approach was used to build several databases which give some hints on the emissivity range and spectral variations for specific materials (see for example [10], [11], [12]).
The indirect reflectance approach will not be dealt in this presentation. We will rather review the approaches that consist in *simultaneously* evaluating the temperature and the emissivity, or that manage to get rid of the emissivity in the procedure of measurement of the temperature.
Even though some of the methods that will be presented later can also apply to the case described by eq. (16) or (17) in which the downwelling radiance $L^{\downarrow}(\lambda)$ is known from independent measurements or from independent simulations, we will focus in the sequel on the cases where the most important contribution to the sensed signal is the surface self-emitted radiation, whereas the reflection contribution can be neglected. Pyrometry of high temperature surfaces with (relatively) cold surrounding surfaces is a typical example.
After a calibration of the optic instrument operating in a narrow spectral band around wavelength λ, we have access to the emitted radiance $L(\lambda,T)$ through the signal S_λ (albeit corrupted by a random noise e_λ):

$$\begin{aligned} S_\lambda &= L(\lambda,T)+e_\lambda \\ &= \varepsilon(\lambda)B(\lambda,T)+e_\lambda \end{aligned} \tag{18}$$

In the field of pyrometry, different methods were devised depending on the number of wavelengths (i.e. spectral bands) used for the measurement: monochromatic pyrometry (§ 3), bispectral pyrometry (§ 4), and multiwavelength pyrometry (§ 5).

3. Single-color or monochromatic pyrometry

Let us first consider that the monochromatic measurement described in eq. (18) is errorless:

$$\begin{aligned} S_\lambda &= L(\lambda,T) \\ &= \varepsilon(\lambda)B(\lambda,T) \end{aligned} \tag{19}$$

An estimation of the surface emissivity then allows inferring the surface temperature. This estimation can be based on prior reflectance measurements or it can be extracted from databases. The question is then: what is the consequence of an emissivity error on the temperature evaluation?
By differentiating eq. (20) we can evaluate the sensitivity of the temperature estimation to an error on the emissivity:

$$\frac{dT}{T} = -\left(\frac{T}{B}\frac{dB}{dT}\right)^{-1}\frac{d\varepsilon}{\varepsilon} \tag{20}$$

The amplification factor $\left(\frac{T}{B}\frac{dB}{dT}\right)^{-1}$ can be easily deduced from the relative sensitivity $\frac{1}{B}\frac{dB}{dT}$ drawn in figure 2.
Also, with the Wien's approximation, equation (20) reduces to :

$$\frac{dT}{T} = -\frac{\lambda T}{C_2}\frac{d\varepsilon}{\varepsilon} \tag{21}$$

The amplification factor is about 0.08 for a temperature of 1100K and at 1µm. It reaches about 0.2 for a temperature of 300K and at 10µm. A 10% underestimation of emissivity will thus lead to a 0.8% overestimation of temperature in the first case (i.e. 8K) and a 2% overestimation in the second case (i.e. 6K). As seen in eq. (21) the error amplification is proportional to λ. The advantage of working at short wavelength is thus evident. For this reason, some authors recommended to apply pyrometry in the visible spectrum or even in the UV spectrum (see for example [13], [14], [15]). However, although a given relative error on emissivity has a lower impact on the temperature estimation when applied at short wavelength, it should not occult the fact that a reasonable estimation of emissivity is anyway needed. The retrieved temperature is unavoidably affected by this (possibly rough) estimation of emissivity [16]. In addition, at short wavelength, both the signal and its *absolute* sensitivity to temperature decrease. The choice of the spectral range for pyrometry is thus always a compromise.

4. Two-Color pyrometry

By performing a measurement at another wavelength, we obtain new information, but unfortunately, we also introduce a new unknown, namely the spectral emissivity at this supplementary wavelength. We thus have at hand two signal values, S_1 and S_1, but three unknowns: temperature T and the two emissivity values $\varepsilon(\lambda_1)$ and $\varepsilon(\lambda_2)$. Assuming errorless signals, we have:

$$\begin{cases} S_1 = L(\lambda_1, T) = \varepsilon(\lambda_1) B(\lambda_1, T) \\ S_2 = L(\lambda_2, T) = \varepsilon(\lambda_2) B(\lambda_2, T) \end{cases} \tag{22}$$

The most popular method consists in calculating the ratio of the two spectral signals (*Ratio two-color pyrometry*):

$$R_{12} = \frac{S_1}{S_2} = \frac{\varepsilon(\lambda_1)}{\varepsilon(\lambda_2)}\frac{B(\lambda_1, T)}{B(\lambda_2, T)} = \frac{\varepsilon(\lambda_1)}{\varepsilon(\lambda_2)}\left(\frac{\lambda_2}{\lambda_1}\right)^5 \frac{\exp(C_2/\lambda_2 T) - 1}{\exp(C_2/\lambda_1 T) - 1} \tag{23}$$

which gives, with the Wien's approximation :

$$R_{12} \approx \frac{\varepsilon(\lambda_1)}{\varepsilon(\lambda_2)}\left(\frac{\lambda_2}{\lambda_1}\right)^5 \exp(-C_2/\lambda_{12} T) = \frac{\varepsilon(\lambda_1)}{\varepsilon(\lambda_2)}\left(\frac{\lambda_2}{\lambda_1}\lambda_{12}\right)^5 \frac{1}{C_1} B_W(\lambda_{12}, T) \tag{24}$$

where the equivalent wavelength λ_{12} of the two-color sensor is defined by :

$$\lambda_{12}{}^{-1} = \lambda_1{}^{-1} - \lambda_2{}^{-1} \quad \Rightarrow \quad \lambda_{12} = \frac{\lambda_1 \lambda_2}{\lambda_2 - \lambda_1} \tag{25}$$

Ratio two-color pyrometry thus requires knowing the emissivity ratio $\varepsilon(\lambda_1)/\varepsilon(\lambda_2)$ in order to infer temperature from the radiance ratio R_{12} according to equation (23) or according to its approximation, equation (24). A common assumption is that emissivity is equal at both wavelengths: $\varepsilon(\lambda_1) = \varepsilon(\lambda_2)$ (it is abusively called the *greybody* assumption even though only the two emissivity values at λ_1 and at λ_2 are required to be equal).
Like for one-color pyrometry, it is easy to relate the temperature estimation error to the emissivity error made at each wavelength:

$$\frac{dT}{T} = -\frac{\lambda_{12} T}{C_2}\left(\frac{d\varepsilon_1}{\varepsilon_1} - \frac{d\varepsilon_2}{\varepsilon_2}\right) \tag{26}$$

Let us consider these two examples defined by the triplets: [T =1100K, $\lambda_1 = 1$µm, $\lambda_2 = 1.5$µm] and [T =300K, $\lambda_1 = 10$µm, $\lambda_2 = 12$µm]. The amplification factor reaches respectively 0.22 and 1.2. These values are 3 and 6 times higher as compared to the examples related to single-color pyrometry in the previous paragraph. The sensitivity of temperature on an error on emissivity is thus far higher with *two-color* pyrometry than with *single color* pyrometry.
The error on temperature can be lowered by reducing the equivalent wavelength λ_{12}, i.e. by increasing the difference between $\lambda_2{}^{-1}$ and $\lambda_1{}^{-1}$, as for example by increasing the higher wavelength λ_2 or decreasing the shorter one λ_1. In any case, the amplification factor will always be larger than the one obtained with single-color pyrometry performed at the shortest wavelength.
A common idea is that by choosing very close wavelengths, the assumption that $\varepsilon(\lambda_1) = \varepsilon(\lambda_2)$ is better justified. However, in doing so, the equivalent wavelength λ_{12} increases and the sensitivity of the radiance ratio to temperature drops dramatically. These conflicting consequences can be solved in the following way. An alternative strategy is to broaden the spectral width, more precisely to increase the $\lambda_1{}^{-1}$ - $\lambda_2{}^{-1}$ difference, (i.e. to decrease λ_{12}). Accordingly, the emissivity ratio $\varepsilon(\lambda_1)/\varepsilon(\lambda_2)$ is then likely to be far from one. A prior knowledge of the ratio $\varepsilon(\lambda_1)/\varepsilon(\lambda_2)$ is thus required for evaluating T from eq. (23) or eq. (24). If this prior estimation of the ratio $\varepsilon(\lambda_1)/\varepsilon(\lambda_2)$ is reliable, the overall benefit of this procedure is that the sensitivity of the radiance ratio to temperature will be higher than before (since the equivalent wavelength λ_{12} will be lower).
With single-color pyrometry performed at λ_1, the required prior knowledge is about $\varepsilon(\lambda_1)$. With (ratio) two-color pyrometry performed at λ_1 and λ_2, the required prior knowledge is about the ratio $\varepsilon(\lambda_1)/\varepsilon(\lambda_2)$. Obviously we cannot escape the introduction of some knowledge about emissivity. However, the advantage as compared to one-color pyrometry is that thanks to the signal ratioing, the method is insensitive to problems like a partial occultation of the

line of sight, or an optical path transmission variation (provided that this transmission variation is the same in both spectral bands).

To evaluate the emissivity ratio $\varepsilon(\lambda_1)/\varepsilon(\lambda_2)$ we could resort to pyroreflectometry [17]-[19]. Each emissivity is equal to $\varepsilon(\lambda,\theta,\varphi)=1-\rho^{\cap'}(\lambda,\theta,\varphi)=1-\pi\eta\rho^{"}(\lambda,\theta_i,\varphi_i,\theta,\varphi)$ where $\rho^{"}(\lambda,\theta_i,\varphi_i,\theta,\varphi)$ is the spectral bidirectional reflectance for incident direction (θ_i,φ_i) and output direction (θ,φ), and η is a diffusion factor related to both directions. The bidirectional reflectance $\rho^{"}(\lambda,\theta_i,\varphi_i,\theta,\varphi)$ is measured at both wavelengths with the use of an additional radiation source (as for example two laser beams at wavelengths λ_1 and λ_2). It is then assumed that the diffusion factor η is wavelength independent. This remaining unknown parameter is finally adjusted until the color temperatures at both wavelengths (together eventually with the ratio temperature) are made coincident. This common temperature is the true one.

In some circumstances, it may be possible to bring close to the object under study a highly reflecting surface (cold mirror). By properly choosing its shape, we obtain two benefits: first the spurious reflections from the environment are diminished, and then the apparent emissivity of the sensed surface is increased thanks to the multiple reflections of the emitted radiation between the surface and the mirror [19]. As a consequence, the temperature estimation error due to errors on emissivity now involves the ratio $\hat{\varepsilon}(\lambda_1)/\hat{\varepsilon}(\lambda_2)$ where $\hat{\varepsilon}$ is the apparent, actually amplified, emissivity (see eq. (24)). Since the ratio $\hat{\varepsilon}(\lambda_1)/\hat{\varepsilon}(\lambda_2)$ is closer to 1 the sensitivity of the temperature evaluation to the errors in emissivity estimation is therefore diminished.
Instead of evaluating the temperature from the radiance ratio in eq. (23) or eq. (24), we could get it from a least-squares minimization between the measured radiances on one side, namely S_1 at λ_1 and S_2 at λ_2 as described in eq. (18), and their theoretical counterparts on the other side. The cost function then expresses as:

$$J(T,\varepsilon(\lambda_1),\varepsilon(\lambda_2))=[S_1-\varepsilon(\lambda_1)B(\lambda_1,T)]^2+[S_2-\varepsilon(\lambda_2)B(\lambda_2,T)]^2 \tag{27}$$

and we are looking for the temperature and emissivity values that minimize this cost function, i.e.:

$$(T,\varepsilon(\lambda_1),\varepsilon(\lambda_2))=\underset{T,\varepsilon(\lambda_1),\varepsilon(\lambda_2)}{\arg\min}\ J(T,\varepsilon(\lambda_1),\varepsilon(\lambda_2)) \tag{28}$$

This corresponds to the OLS (ordinary least-squares) method, however here, the problem is underdetermined since, as said before, there are three unknown parameters: T, $\varepsilon(\lambda_1)$ and $\varepsilon(\lambda_2)$ and only two observations: S_1 and S_2. One way to solve it is to introduce a functional relationship between the two emissivity values. With this new constraint, the number of unknowns is reduced by one. An example of such a relationship is obtained by specifying a value β for their ratio:

$$\varepsilon(\lambda_1)/\varepsilon(\lambda_2)=\beta \tag{29}$$

This statement of constant emissivity-ratio is shared with the ratio method for pyrometry already invoked (see eq. (23)). We then have two methods for evaluating the temperature from the two spectral signals S_1 and S_2: either from their ratio in eq. (23) of from the least squares equation in eq. (27)-(28). The signals are actually corrupted by an additive random experimental noise and it is known that the expected value of the ratio is a biased estimator of the ratio of the expected values. It is thus better to use eq. (27)-(28) for the temperature identification.
Many other functional relationships could be used. Here are a few examples:

$$\varepsilon(\lambda_1) - \varepsilon(\lambda_2) = \beta \tag{30}$$

$$1/\varepsilon(\lambda_1) - 1/\varepsilon(\lambda_2) = \beta \tag{31}$$

where β is a material-dependent constant whose value should be provided.
The emissivity compensation methods of Foley [21], Watari [22] and Anderson [23] described in [24] can all be connected to the following general relationship:

$$\varepsilon(\lambda_1) = \varepsilon(\lambda_2)^{\beta} \tag{32}$$

where again β is a material-dependent constant (in [22] it was actually fixed to λ_1/λ_2).
The crucial point with two-color pyrometry is to find out a functional relationship like those in eq. (29) to eq. (32) together with the value of the associated parameter β. It often happens that a good choice for a given material may lead to poor results for another material or for the same material in a different state (oxidation, ageing). The great difficulty, when dealing with different materials or materials of different states, consists in finding a general functional relation capable of representing all the observed spectral variations of the emissivity.

5. Multiwavelength pyrometry

We can proceed further by adding measurements performed at additional wavelengths. In the end, we come with m values of spectral signal S_i, $i = 1,...,m$ which correspond to experimental measurements of m values of the spectral radiance $L(\lambda_i, T)$, $i = 1,...,m$. Each of these measurements is contaminated by a random error e_i, $i = 1,...,m$:

$$\begin{aligned} S_i &= L(\lambda_i, T) + e_i \\ &= \varepsilon_i B(\lambda_i, T) + e_i \end{aligned} \qquad i = 1,...,m \tag{33}$$

The problem still remains underdetermined since we have at hand m equations (i.e. m radiance measurements), but at the same time, we face $n = m + 1$ unknowns, namely the temperature T and m values of spectral emissivity $\varepsilon_i = \varepsilon(\lambda_i)$, $i = 1,...,m$. The vector of parameters will be called $\boldsymbol{\beta} = (\varepsilon_1 \ ... \ \varepsilon_m \ T)^T$.
Multiwavelength pyrometry has been a subject of controversy for several decades [16], [25]-[52]. The experimental results showed various successes, sometimes with small temperature errors, other times with unacceptably high errors, depending on the material, on its surface

state, and on the function chosen to approximate the emissivity spectrum. Even from the numerous theoretical works on this subject, it is hard to find a consensus about the advantage or not of using many (or possibly a large number of) wavelengths [25], [26], [31], [33], [35], [36], [37], [44], [45], [48]-[53].
In the following we will present a few results which highlight the difficulty to obtain good and repeatable results with some multiwavelength approaches. A series of error mitigation processes will also be described.
In many cases, the problem is addressed by ignoring the presence of experimental errors. As such, the system of equations to solve is:

$$S_i = \varepsilon_i B(\lambda_i, T), \quad i = 1,...,m \tag{34}$$

Of course, the temperature $\hat{T}$ and emissivity values $\hat{\varepsilon}_i$, $i = 1,...,m$ obtained therefrom are different from the real values T and ε_i, $i = 1,...,m$ that yielded the observed signals S_i, $i = 1,...,m$ (actually affected by experimental errors, see eq. (34)). This will be discussed next.
We see from eq. (33) that the problem is non-linear with respect to the parameters. However, when taking the logarithm to the signal and introducing the Wien's approximation to the blackbody radiance, the problem becomes linear with respect to the following transformed parameters $\boldsymbol{\beta} = \left(\ln(\varepsilon_1) ... \ \ln(\varepsilon_m) \ \ T_{ref}/T\right)^T$, where T_{ref} is an arbitrary reference temperature used for scaling the temperature. The new vector of observables will be called $\mathbf{Y} = \left(Y_1 \ ... \ Y_m\right)^T$ and as a first approximation, we will assume that the experimental error affecting the observables Y_i is additive as well (it will be called e_i'):

$$Y_i \equiv \ln\left(S_i \frac{\lambda_i^5}{C_1}\right) = \ln(\varepsilon_i) - \mu_i \frac{T_{ref}}{T} + e_i', \quad i = 1,...,m \tag{35}$$

where μ_i is a constant coefficient multiplying the unknown parameter T_{ref}/T and defined by:

$$\mu_i \equiv \frac{C_2}{\lambda_i T_{ref}}, \quad i = 1,...,m \tag{36}$$

5.1. Interpolation-based methods

To solve the underdetermined problem, a *potential* solution would be to *reduce by just one* the number of degrees of freedom related to the spectral emissivity data. In other words, instead of considering m unknown free parameters ε_i, $i = 1,...,m$, the emissivity values ε_i should be described by a parametric function based on $m-1$ parameters only. Several such emissivity models were proposed in the past. A polynomial of degree $m-2$ has often been considered:

$$\varepsilon_i = \sum_{j=0}^{m-2} a_j \lambda_i^{\ j}, \quad i = 1,...,m \tag{37}$$

The same could be done for the logarithm of emissivity when using the linearized version in eq. (35):

$$\ln(\varepsilon_i) = \sum_{j=0}^{m-2} a_j \lambda_i{}^j, \qquad i = 1,...,m \tag{38}$$

In both cases, the remaining $m-1$ free parameters are the $m-1$ coefficients of the polynomial: $a_j \quad j = 0,...,m-2$.

However, it was shown in [26], based on the Wien's approximation (eq. (35)) and a polynomial representation of $\ln(\varepsilon_i)$ (eq. (38)) that this method can rapidly lead to unrealistic temperature values as m increases.

Let us first assume that there is no measurement error, i.e. $e_i' = 0$, $i = 1,...,m$ in eq. (35):

$$Y_i = \ln(\varepsilon_i) - \mu_i \frac{T_{ref}}{T}, \quad i = 1,...,m \tag{39}$$

Upon considering the polynomial representation of degree $m-2$ for $\ln(\varepsilon_i)$ in eq. (38), the system of m equations is now based on m unknowns only. However, the introduction of the emissivity model has the consequence that the estimated temperature T' obtained by solving the linear system of equations is different from the real temperature T. The estimated temperature T' satisfies:

$$Y_i = \sum_{j=0}^{m-2} a_j \lambda_i{}^j - \mu_i \frac{T_{ref}}{T'}, \quad i = 1,...,m \tag{40}$$

By multiplying eq. (40) by λ_i, we obtain:

$$\lambda_i Y_i = \sum_{j=1}^{m-1} a_j \lambda_i{}^j - \frac{C_2}{T'}, \quad i = 1,...,m \tag{41}$$

which shows that $-C_2/T'$ corresponds to the constant parameter of the polynomial of degree $m-1$ interpolating the m values $\lambda_i Y_i$.

We can also notice (by subtracting eq. (41) from eq. (39) multiplied by λ_i) that the temperature error expressed through $C_2(1/T - 1/T')$ (it has also been called "temperature correction") corresponds to the constant parameter of the polynomial of degree $m-1$ interpolating the m values $\lambda_i \ln(\varepsilon_i)$:

$$\lambda_i \ln(\varepsilon_i) = \sum_{j=1}^{m-1} a_j \lambda_i{}^j + C_2\left(\frac{1}{T} - \frac{1}{T'}\right) \qquad i = 1,...,m \tag{42}$$

As a consequence, the temperature correction for single color, bicolor and tricolor pyrometry (m =1,2,3) is expressed by [16], [34]:

$$
\begin{aligned}
m=1 \qquad & C_2\left(\frac{1}{T}-\frac{1}{T'}\right)=\lambda_1 \ln(\varepsilon_1) \\
m=2 \qquad & C_2\left(\frac{1}{T}-\frac{1}{T'}\right)=\frac{\lambda_1\lambda_2}{\lambda_1-\lambda_2}\ln\left(\frac{\varepsilon_2}{\varepsilon_1}\right) \\
m=3 \qquad & C_2\left(\frac{1}{T}-\frac{1}{T'}\right)=\frac{\lambda_1\lambda_2\lambda_3}{(\lambda_2-\lambda_1)(\lambda_3-\lambda_1)(\lambda_3-\lambda_2)}\left(\lambda_1\ln\left(\frac{\varepsilon_2}{\varepsilon_3}\right)+\lambda_2\ln\left(\frac{\varepsilon_3}{\varepsilon_1}\right)+\lambda_3\ln\left(\frac{\varepsilon_1}{\varepsilon_2}\right)\right)
\end{aligned}
\tag{43}
$$

The temperature correction involves the ratio $\varepsilon_1/\varepsilon_2$ for m=2. With equidistant wavelengths, it involves the ratio $\varepsilon_1\varepsilon_3/\varepsilon_2^{\,2}$ for m=3 and the ratio $\varepsilon_1\varepsilon_3^{\,2}/\varepsilon_2^{\,2}\varepsilon_4$ for m=4 [34]. These ratios are of course to estimate beforehand. Assigning arbitrarily a value of 1 to the emissivity ratio for a series of metals had the consequence that the temperature estimation error increased very rapidly with the number of wavelengths [34].
It can be shown that the temperature correction limit for wavelength intervals decreasing to 0 is equal to $(-1)^{m-1}\lambda^m/(m-1)!d^{m-1}\ln[\varepsilon(\lambda)]/d\lambda^{m-1}$ [31].
We can also recognize in eq. (42) that the temperature correction corresponds to the extrapolation at $\lambda=0$ of the polynomial of degree $m-1$ used to interpolate the m values $\lambda_i \ln(\varepsilon_i)$. This finding can now be developed a little more. If, *by chance*, a polynomial of degree $m-2$ could be found passing *exactly* through the m values $\ln(\varepsilon_i)$, the polynomial of degree $m-1$ passing through the m values $\lambda_i \ln(\varepsilon_i)$ would then correspond to the previous polynomial function multiplied by λ. The constant parameter (i.e. the temperature correction term) would thus be equal to 0. As a consequence, the estimated temperature would be the exact one. However, in reality, that a polynomial of degree $m-2$ could be found passing *exactly* through the m values $\ln(\varepsilon_i)$ is highly improbable. Therefore, in practice, there is an unavoidable error regarding temperature. In addition, the error magnitude is tightly dependent on the properties of polynomial *extrapolation*. Unfortunately it is well known that using a polynomial interpolation to perform an extrapolation leads to increasingly high errors as the polynomial degree rises. Furthermore, things get progressively worse as the extrapolation is done far from the interpolation interval. Since the aforementioned extrapolation is done at $\lambda=0$, this last point would actually advocate expanding the spectral range to the shortest possible wavelength (whose consequence would be to bring the extrapolation point closer to the interpolation interval), but this is only a desperate remedy.

The potentially catastrophic errors described just before are actually systematic errors, namely method errors. They are obtained even when assuming errorless spectral signals. To analyze the influence of the measurement errors, we can state, for ease, that the measurement error in channel i has the same impact as a corresponding uncertainty of the emissivity in the same channel, namely $d\varepsilon_i$. Then, the interpolation of the transformed values $\lambda_i \ln[\varepsilon_i + d\varepsilon_i]$ leads to the same nature of extrapolation errors as described before. Finally both extrapolation errors add together. The calculated temperature is thus more and more sensitive to measurement errors as the number of spectral bands increases.
The poor success of the *interpolation based* method originates from what has been called an *over-fitting* of the experimental data. It was finally recognized that the *interpolation based*

method could be considered but only for the simpler pyrometers, actually with two or three wavelengths at most [26].

5.2. Regularization by using a low-order emissivity model

5.2.1. Emissivity models

The shortcomings of the over-fitting previously described can be mitigated by reducing the number of unknown used to describe the emissivity spectrum.
Different models were tested in the past:

$$\varepsilon_i = \sum_{j=0}^{k} a_j \lambda_i{}^j \; ; \qquad i = 1,...,m \; ; \qquad k < m-2 \quad \text{(generally } k\text{=1 or 2)} \tag{44}$$

$$\ln(\varepsilon_i) = \sum_{j=0}^{k} a_j \lambda_i{}^j \; ; \qquad i = 1,...,m \; ; \quad k < m-2 \quad \text{(generally } k \text{ =1 or 2)} \tag{45}$$

$$\varepsilon_i = 1/\left(1 + a_0 \lambda_i{}^2\right); \qquad i = 1,...,m \tag{46}$$

Besides that, models of $\ln(\varepsilon_i)$ based on polynomials of the variable $\lambda_i{}^{1/2}$ or $\lambda_i{}^{-1/2}$ and models involving the brightness temperature were considered in [44], [45]. A sinusoidal function of λ_i in [25], and other more "physical" models like Maxwell, Hagen-Rubens and Edwards models were presented in [16], [38], [48].
Since the aim is merely to parameterize the m spectral values of emissivity with the help of only m_p parameters with $m_p < m-1$, there is no limit to the fertility of ideas spawned by pyrometrists to find new models. Indeed, new "analytical" model are constantly being published (see e.g. [41]-[52]), without the results being up to expectations, and for good reasons, as shown later.
On the other side, the grey-band model consists in splitting the spectrum into a small number of bands m_b, with $m_b < m$, and assigning the same emissivity value to all wavelengths λ_i belonging to a given band [33]. In this way, the number of unknowns is reduced from $m+1$ to m_b+1. The bands can be narrowed to contain only three or two spectral channels as suggested in [76]. We can go even further by squeezing some bands to merely one spectral channel. The extreme limit consists in $m-1$ single-channel bands plus one dual-channel band. In that case we face a problem with m measurements and m unknowns which is thus, *in principle*, invertible. We will see that it is actually very badly conditioned.
The concept of grey-bands can be generalized by allowing that the channels that are chosen to share a common emissivity value are not necessarily close together: an iterative process was described in [50] where these wavelengths are each time reshuffled according to the pseudo-continuous emissivity spectrum, i.e. the one defined over the m wavelengths λ_i according to:

$$\hat{\varepsilon}\left(\lambda_i,\hat{T}\right)=\frac{L(\lambda_i,T)}{B\left(\lambda_i,\hat{T}\right)} \qquad i=1,...,m \tag{47}$$

where $\hat{T}$ is the most recent temperature estimation. $\hat{\varepsilon}\left(\lambda_i,\hat{T}\right)$ is sorted from lower to higher values and the m_b bands of equal emissivity values are defined by splitting the $\hat{\varepsilon}\left(\lambda_i,\hat{T}\right)$ vector into m_b parts.

The unknown parameters of the emissivity function, together with temperature, are finally evaluated by least squares minimization. The simplest way consists in introducing the Wien approximation to express the blackbody radiance and considering the observable $Y_i=\ln\left[S_i\,\lambda_i^{\,5}/C_1\right]$, see eq. (35). The logarithm of the emissivity values and the inverse of temperature (or T_{ref}/T) act as parameters of the linear model. Then, by introducing a polynomial approximation for $\ln(\varepsilon_i)$ (see eq. (38)) but of degree $k<m-2$, we come to a system of m equations:

$$Y_i=\sum_{j=0}^{k}a_j\lambda_i^{\,j}-\mu_i\frac{T_{ref}}{T}+e_i',\quad i=1,...,m \tag{48}$$

and the problem now reduces to an estimation of the linear parameters a_j, $j=0,...,k$ and T_{ref}/T. This was done by a *linear least squares* method in ([25], [30], [42], [43]).

Otherwise, when taking for the observable the spectral signal S_i itself, we face a *non-linear least squares* problem ([27], [29], [32], [33], [35]-[41], [43]-[48], [51], [53]).

Let us add that by rearranging the m equations as described in eq. (35) we could get rid of one parameter, either a constant parameter or the temperature ([25], [30], [43]). However it is believed that no advantage in accuracy is expected by manipulating the data to present the same information in a different form [25]. As a matter of fact, in the case of linear fitting, such a manipulation even increases the estimation error of the identified parameters.

We will now consider different aspects of the Least Squares Multiwavelength Pyrometry solution (LSMWP).

5.2.2. Least-squares solution of the linearized Temperature Emissivity Separation problem (TES)

We will adopt the Wien's approximation and consider the vector of observables vector of observables $\mathbf{Y}=(Y_1\ ...\ Y_m)^T$ described in eq. (35). We will assume here that the experimental errors e_i', $i=1,...,m$ are uncorrelated random variables following a Gaussian distribution of uniform variance. It is usually assumed that the spectral signal S_i, not the compound logarithm Y_i in eq. (35), is affected by a noise of uniform variance. The present approximation is valid if the spectral range is not too wide with respect to the shape of the Planck's law $B(\lambda,T)$ and if the emissivity values don't span a too wide interval. Otherwise a Maximum Likelihood Estimation (MLE) is better appropriate.

According to equation (38) where $\ln(\varepsilon_i)$ is approximated by a polynomial of degree $k < m-2$, the least squares solution is:

$$\hat{\boldsymbol{\beta}} = \left[\hat{a}_0 \quad ... \quad \hat{a}_k \quad \frac{1}{\hat{T}} \right]^T = \underset{a_j, T}{\arg Min} \sum_{i=1}^{m} \left(Y_i - \left(\sum_{j=0}^{k} a_j {\lambda_i}^j - \frac{C_2}{\lambda_i T} \right) \right)^2 \tag{49}$$

For numerical reasons (the reason is not only to manipulate numbers that are of similar range, but to minimize a particular condition number, see later), it is preferable to replace the wavelength λ_i in the polynomial expression by its reduced and centered value $\lambda_i *$ defined by:

$$\lambda_i * = 2 \frac{\lambda_i - \lambda_{\min}}{\lambda_{\max} - \lambda_{\min}} - 1 \tag{50}$$

In this way $\lambda_i * \in [-1,1]$. For the same reason, it is better to normalize T by T_{ref} where T_{ref} is chosen in such a way that the coefficients $\mu_i \equiv C_2 / \lambda_i T_{ref}$ (see eq. (36)) are of the order of 1. The associated unknown parameter is then $\beta_T * = T_{ref} / T$. The parameter vector is:

$$\hat{\boldsymbol{\beta}} * = \left[\hat{a}_0 * \quad ... \quad \hat{a}_k * \quad \frac{T_{ref}}{\hat{T}} \right]^T = \underset{a_j *, T}{\arg Min} \sum_{i=1}^{m} \left(Y_i - \left(\sum_{j=0}^{k} a_j * {\lambda_i *}^j - \mu_i \frac{T_{ref}}{T} \right) \right)^2 \tag{51}$$

where the parameters $a_j *$ are the coefficients of the polynomial expressed in terms of $\lambda_i *$. The sensitivity matrix of this linear model is the following $m \times (k+2)$ matrix:

$$\mathbf{X} = \begin{bmatrix} 1 & \lambda_1 * & {\lambda_1 *}^2 & ... & -\mu_1 \\ ... & ... & ... & ... & ... \\ 1 & \lambda_m * & {\lambda_m *}^2 & ... & -\mu_m \end{bmatrix}_{m,k+2} \tag{52}$$

where the columns correspond to the sensitivity to any of the $k+2$ parameters present in vector $\boldsymbol{\beta} *$ (i.e. the first derivative of the model function relatively to each parameter).

The sensitivities to the first three parameters $a_j *$ ($j = 0,..2$) and to $\beta_T *$ have been plotted vs. the reduced wavelength $\lambda *$ in figure 3 for the particular case $\lambda_{\max} / \lambda_{\min}$ =5/3. The absolute values of the wavelength are not important, only the relative width of the total spectral band is relevant (the spectral interval [3µm-5µm] satisfies the present criterion on relative width, $\lambda_{\max} / \lambda_{\min}$ =5/3).

The sensitivity to the first three coefficients of the model are respectively a constant, a linear and a quadratic function of the reduced wavelength $\lambda *$. The important question is how the sensitivity to the temperature reciprocal does compare to the former sensitivity functions? It is actually very smooth, close to linear. We thus expect a strong correlation between the parameters (since the sensitivity vectors are nearly collinear).

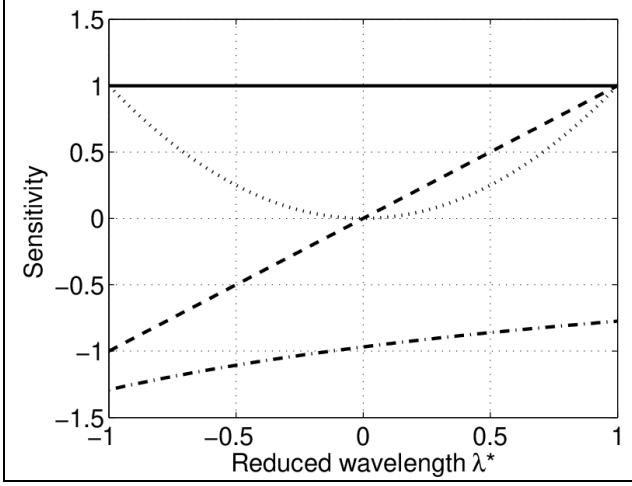

Figure 3. Sensitivity to the first three coefficients of the polynomial model (resp. continuous, dashed and dotted line) and to the inverse of the normalized temperature (dashed-dotted line). The reduced wavelength is λ^* (see eq. (50)). For this illustration, the total spectral interval is such that $\lambda_{\max}/\lambda_{\min}$ =5/3.

The estimator of the parameter vector $\hat{\boldsymbol{\beta}}^*$ based on the OLS method is obtained by solving the $m \times m$ linear system (see the lecture devoted to linear estimation):

$$\left(\mathbf{X}^T\mathbf{X}\right)\hat{\boldsymbol{\beta}}^* = \mathbf{X}^T\mathbf{Y} \tag{53}$$

The fact that the sensitivities are nearly dependent leads to a $\mathbf{X}^T\mathbf{X}$ matrix that is near-singular. Indeed, by computing the condition number of the matrix $\mathbf{X}^T\mathbf{X}$ (the condition number is the ratio between the maximum and minimum eigenvalues), we obtain very high values, even when the polynomial model has a low degree (see figure 4). The condition number increases exponentially with the polynomial degree (it increases by a factor of about 100 when the polynomial degree is increased by just one). Furthermore, this figure shows that increasing the number of spectral measurements in a given spectral interval brings no improvement regarding the condition number. Notice also that if the normalizations described in eq. (49) and (50) were not applied, the condition number would reach even higher values.
The condition number describes somehow the rate at which the identified parameters will change with respect to a change in the observable; indeed it measures the sensitivity of the solution of a system of linear equations to errors in the data. Hence, if the condition number is large, even a small error in the observables may cause a large error in the identified parameters (the condition number however only provides an upper bound). The condition number also reflects how a small change in the matrix $\mathbf{X}^T\mathbf{X}$ itself will affect the identified parameters. Such a change may be due to the measurement error of the equivalent wavelength corresponding to each spectral channel. From figure 4, a first statement is that the regularization with a polynomial model of degree 2 or higher will not be efficient. But even a polynomial model of degree 1 is expected to show unstable results (the condition number is in this case of about 10^4.

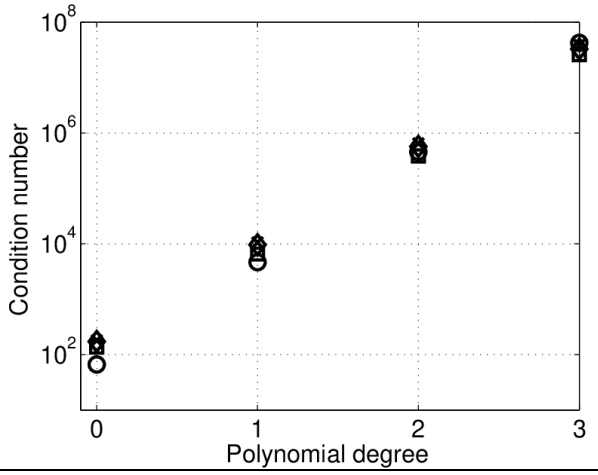

Figure 4. Condition number of the matrix $\mathbf{X}^T\mathbf{X}$ versus the polynomial degree k of the emissivity model and for a number of spectral measurements equal to $m = k + 2$ (○), m =7 (□), m =30 (◊), m =100 (x). For this illustration, the total spectral interval is such that $\lambda_{\max}/\lambda_{\min}$ =5/3.
The case $m = k + 2$ is the limiting case avoiding under-determination (§5.1).

The condition number has been computed in [3] for a larger spectral interval, namely for the case $\lambda_{\max}/\lambda_{\min}$ =1.75 (the interval [8µm-14µm] satisfies this criterion regarding the relative width). It was found slightly lower as compared to the present values. Increasing the relative width of the total spectral band is thus beneficial from this point of view.

However, the condition number is not all. Sometimes it could even be misleading because it only gives an upper bound of the error propagation. It is indeed better to analyze the diagonal values of the covariance matrix $\left(\mathbf{X}^T\mathbf{X}\right)^{-1}$. They actually provide the variance amplification factor for each identified parameter $P*$:

$$\left[\sigma_{\boldsymbol{\beta}^*}{}^2\right] = diag\left(\left(\mathbf{X}^T\mathbf{X}\right)^{-1}\right)\sigma^2 \tag{54}$$

where σ^2 is the variance of the observable Y_i, i.e. $\left(\sigma_{S_i}/S_i\right)^2$ which is here assumed independent of the spectral channel i (if instead one assumes that the radiance variance $\left(\sigma_{S_i}\right)^2$ is uniform, the result would be $\left[\sigma_{\boldsymbol{\beta}^*}{}^2\right] = diag\left(\left(\mathbf{X}^T\boldsymbol{\Psi}^{-1}\mathbf{X}\right)^{-1}\right)$ where $\boldsymbol{\Psi}$ is the covariance matrix of the observable Y_i).
One should be aware that $\sigma_{\boldsymbol{\beta}^*}{}^2$ merely describes the error around the mean estimator value due to the radiance error propagation to the parameters. If the mean estimator is biased, as it is the case when the true emissivity profile is not well represented by the chosen model, we should add the square *systematic error* to obtain the RMS error. The latter better represents the misfit to the true parameter value, either the temperature or a spectral emissivity value (this will be described later through a Monte-Carlo analysis of the inversion process).
With the polynomial model, the mean standard relative error for emissivity, which is defined by:

$$\frac{\sigma_\varepsilon}{\varepsilon} \equiv \sqrt{\frac{1}{m}\sum_{i=1}^{m}\frac{\sigma_{\varepsilon_i}{}^2}{\varepsilon_i{}^2}} \tag{55}$$

is related to the standard error of the retrieved polynomial coefficients through:

$$\frac{\sigma_\varepsilon}{\varepsilon} = \sqrt{\frac{1}{m}\sum_{i=1}^{m}\left[X_{ij}{}^2\right]^T\left[\sigma_{a_j*}{}^2\right]_{j=1,k}} \tag{56}$$

As such, it can be related to the uncertainty of the observable σ_Y (which corresponds to σ_S/S) through an error-amplification factor K_ε:

$$\frac{\sigma_\varepsilon}{\varepsilon} = K_\varepsilon \frac{\sigma_S}{S} \tag{57}$$

With the grey-bands model, the mean standard error and the amplification factor K_ε are defined according to:

$$\frac{\sigma_\varepsilon}{\varepsilon} \equiv \sqrt{\frac{1}{m}\sum_{i=1}^{m_b}\left(\frac{\sigma_{\varepsilon_i}}{\varepsilon_i}\right)^2} = K_\varepsilon \frac{\sigma_S}{S} \tag{58}$$

From the Wien's expression of the blackbody radiance, it is clear that the standard relative error for temperature is proportional to the temperature, to σ_S/S, and to a wavelength scale $\tilde{\lambda}$ representative of the spectral window (we can choose the geometric mean of the window limits: $\tilde{\lambda} \equiv \sqrt{\lambda_{\min}\lambda_{\max}}$). The error amplification factor for the temperature, K_T, is thus defined through:

$$\frac{\sigma_T}{T} = K_T \tilde{\lambda} T \frac{\sigma_S}{S} \tag{59}$$

The error amplification factors K_T and K_ε have been plotted in figure 5 versus the degree of the polynomial model of emissivity, assuming again a relative bandwidth $\lambda_{\max}/\lambda_{\min}$ of 5/3.
A first comment is that the standard errors increase exponentially with the polynomial degree k. The rise is roughly like $\exp(2k)$. The amplification factors can be reduced somewhat by widening the spectral window; in addition, the increasing rate with the polynomial degree is lower (compare with the results in [3] obtained for $\lambda_{\max}/\lambda_{\min}$ =1.75).
With the grey-bands model, the standard errors increase nearly in proportion to the number of bands (see [3]).
In both cases, the standard errors decrease with the total number of spectral measurements, roughly like $m^{-1/2}$.

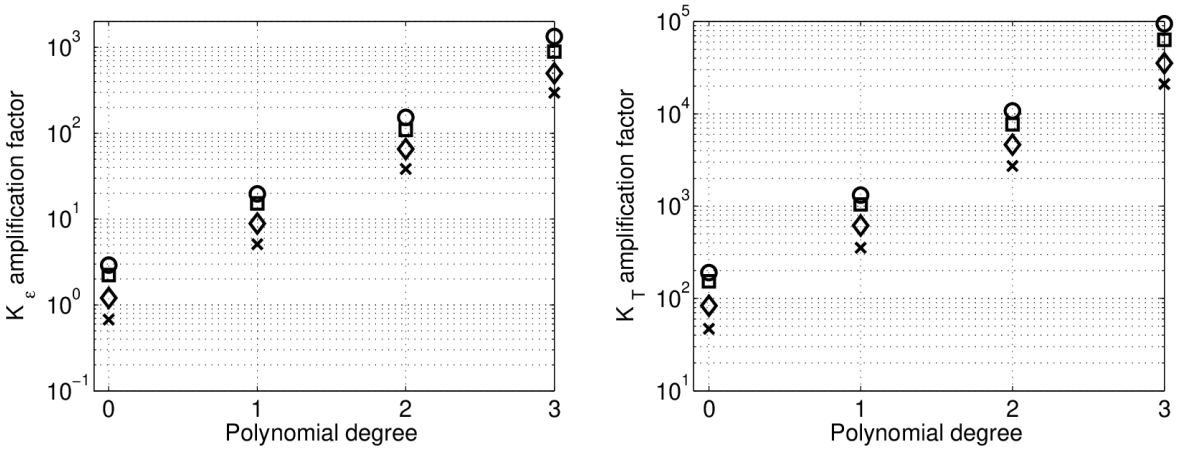

Figure 5: Left : Error amplification factor on emissivity versus the polynomial degree *m* chosen to model $\ln[\varepsilon(\lambda)]$. The symbols correspond to different numbers of spectral measurements: $m = k + 2$ (○), m =7 (□), m =30 (◊), m =100 (x). Right : Same for the error amplification factor on temperature. The case $m = k + 2$ is the limiting case avoiding under-determination.

Regarding the bandwidth influence, let us notice that the relative error on temperature depends both on $\lambda_{\min}$ and $\lambda_{\max}$ whereas the mean relative error on emissivity only depends on the ratio $\lambda_{\max}/\lambda_{\min}$ (for a given value of σ_S/S in eq. (57) and (59)).
Assuming a target at 600K, a pyrometer with seven wavelengths between 3µm and 5µm and 1% radiance noise in each spectral channel, will provide temperature and emissivity values with standard errors as reported in Table 1, depending on the degree of the polynomial chosen to model the logarithm of emissivity $\ln(\varepsilon_i)$.

Table 1. Polynomial model for (the logarithm of) emissivity. Root-mean square error for the estimated temperature and the emissivity depending on the degree of the polynomial model. Target temperature is 600K. Pyrometry performed at seven wavelengths between 3µm and 5µm with 1% radiance noise

Polynomial degree	σ_T (K)	σ_ε
0	2.1	0.02
1	14.5	0.13
2	107.5	1.1

The errors are already high with a linear model and they reach unacceptably high values with a polynomial model of degree two. These results seem to preclude using the least squares linear regression approach with a polynomial model of degree 2 and more.
Notice that these results have been obtained with the use of the Wien's approximation. However, the Planck's law is close to the Wien's approximation over a large spectrum, therefore we expect that the general least squares nonlinear regression based on the Planck's law will also face serious problems when using a polynomial model for emissivity.

Let us recall that the temperature and emissivity errors mentioned above only describe how the radiance errors propagate to the parameters. It has been assumed here that the emissivity spectrum otherwise *perfectly* matches the considered polynomial model. If this is not the case (which actually occurs almost every time) a *systematic error* appears and is added to the previous one. The joint errors will be presented in §5.2.4 through a Monte-Carlo analysis.

Applying the grey-bands model to the previous example leads to the standard errors shown in Table 2. The number of grey-bands can be increased up to $m_b = m - 1 = 6$ (which is the maximum to avoid underdetermination in the considered case of $m = 7$ spectral measurements).

Table 2. Grey-band model for emissivity. Root-mean square error for the estimated temperature and the emissivity depending on the number of grey-bands when assuming $m = 7$ spectral measurements. Target temperature is 600K. Pyrometry is performed at seven wavelengths between 3µm and 5µm with 1% radiance noise.

Number of bands	σ_T (K)	σ_ε
1	2.7	0.02
2	4.9	0.04
3	7.0	0.05
4	10.7	0.08
5	12.6	0.10
6	13.7	0.11

The errors increase with the number of grey-bands, starting from the values corresponding to a degree 0 polynomial and ending at values that are lower than those obtained with a polynomial of degree 1. This is interesting in the sense that even with six grey-bands, i.e. six degrees of freedom for emissivity, the errors don't "explode" as it was observed before by increasing the polynomial degree. The grey-bands model, although not being smooth, could thus capture more easily rapid variations in the emissivity profile like peaks.
However, as stated before, the standard errors that have been presented here only show what happens when noise corrupts the radiance emitted by a surface but assuming that the true emissivity otherwise *perfectly follows the staircase model*. As such, with the 6-bands case, the emissivity should be *equal* in the two channels that were chosen to form the largest grey-band. As this is never strictly the case, again, a *systematic error* will be added to the one shown in Table 2.

5.2.3. Another look on the solutions of the TES problem

Another way of presenting the ill-posedness of the TES problem and the difficulties in finding an appropriate regularization method consists, like in [26], in exposing first the multiple solutions to the underdetermined problem shown in eq. (34). It is clear from this set of equations that when selecting a value $\hat{T}$ for temperature, the emissivity values $\hat{\varepsilon}_i\left(\hat{T}\right)$ obtained from:

$$\hat{\varepsilon}_i\left(\hat{T}\right) = S_i / B\left(\lambda_i, \hat{T}\right), \quad i = 1,...,m \tag{60}$$

are such that, when combined with $\hat{T}$ they provide a *perfect* solution to the problem presented in eq. (34), namely a solution that exactly leads to the observed spectral signals. The emissivity values obtained in this way depend on the selected temperature, which explains the notation $\hat{\varepsilon}_i\left(\hat{T}\right)$. Increasing the value of $\hat{T}$ entails a decrease in all spectral emissivity values and vice versa. There is an infinite number of *exact* sets of solutions $\boldsymbol{\beta} = \left(\hat{\varepsilon}_1\left(\hat{T}\right)... \ \hat{\varepsilon}_m\left(\hat{T}\right) \ \hat{T}\right)^T$, the only limitation is that $\max_{i=1,m} \hat{\varepsilon}_i\left(\hat{T}\right) \le \varepsilon_{\max}$ and $\varepsilon_{\min} \le \min_{i=1,m} \hat{\varepsilon}_i\left(\hat{T}\right)$. The boundary values $\varepsilon_{\min}$ and $\varepsilon_{\max}$ are chosen in accordance with the type of tested materials. Without other information $\varepsilon_{\max}$ is usually set to 1 whereas $\varepsilon_{\min}$ can be set to 0.02 since it is unusual to find surfaces with emissivities less than about 0.02, and these are very clean, polished metal surfaces [26].

As an illustration we considered a multiwavelength system operating over seven narrow spectral bands in the [3µm-5µm] range, excluding the 4.3µm CO2 absorption band of the atmosphere. The central wavelengths are 3, 3.5, 3.7, 4, 4.6, 4.8 and 5 µm. Two hypothetic materials have been considered. The first one presents an emissivity profile such that the seven emissivity values at the former seven wavelengths are distributed perfectly linearly between 0.72 at 3µm and 0.53 at 5µm. The emissivity of the second material has the following values: 0.72, 0.75, 0.63, 0.57, 0.56, 0.51, 0.53 at the former seven wavelengths.
These two emissivity distributions have been represented with circles in figure 6, resp. in figure 7. The spectral radiance has then been computed at the central wavelengths according to the Planck's law, assuming a temperature of 600K. At first no measurement error was considered, it will be added later. The objective was to retrieve from the seven radiance values the true temperature and the true emissivity distribution for both materials.
To start, we selected different values for the temperature $\hat{T}$ between 580K and 660K, and then plotted the distribution of emissivity $\hat{\varepsilon}_i\left(\hat{T}\right)$ that perfectly matches with each value of $\hat{T}$ (curves with star symbols), namely that yields the same seven values of spectral radiance as those observed with the combination of true temperature and true emissivity distribution.
We notice that temperature values $\hat{T}$ as low as about 577K could be acceptable; however, lower temperature values should be discarded since they make one of the emissivity values $\hat{\varepsilon}_i\left(\hat{T}\right)$ larger than one. On the other hand, temperature values $\hat{T}$ much higher than the real temperature of 600K could be well accepted.

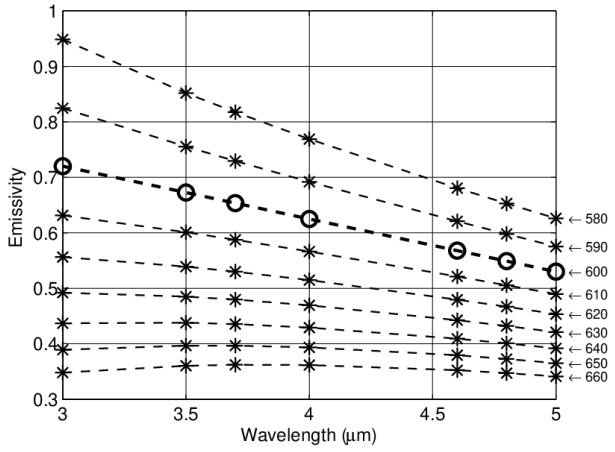

Figure 6. Emissivity profiles inferred from the spectral radiance (at seven wavelengths between 3µm and 5µm) by considering several hypothetical temperature values $\hat{T}$ higher or lower than the "real" temperature T =600K. The temperature values $\hat{T}$ are indicated on the right. The "true" emissivity distribution is with circles; it is here assumed *linear* with the wavelength.

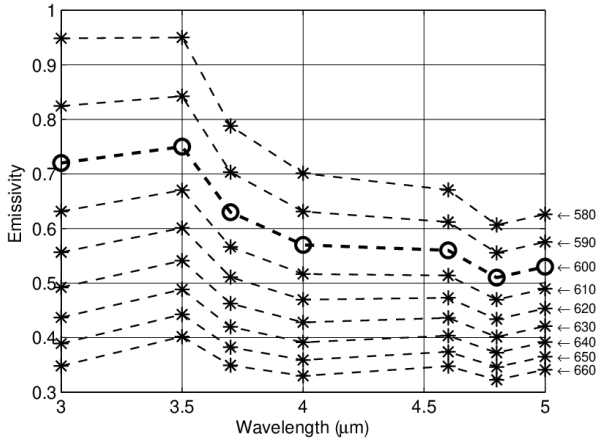

Figure 7. Same as in figure 6 for a *non-linear* emissivity distribution.

The traditional way consists in looking for a distribution of emissivity in the form of a polynomial in wavelength and performing a least-squares regression on the emitted radiance. As an example let us consider a polynomial model of degree 1. In this case, the problem can be reformulated as follows: among all hypothetic emissivity profiles represented in figure 6 (respectively in figure 7 for the second material), *which one is closest to a straight line* ?

Let us give some indications on this notion of closeness. It is quantified by the sum of the square residues between any emissivity distribution in fig. 6 or 7 and the straight line obtained by linear regression. We are actually dealing with weighted least squares: each term should be weighted by the blackbody radiance expressed at the corresponding temperature $\hat{T}$. Hence, let us consider the weighted linear regression of a particular distribution $\hat{\varepsilon}_i\left(\hat{T}\right)$; the considered weight is $B\left(\lambda_i,\hat{T}\right)$. The sum of square residues is:

$$R^2\left(\hat{T}\right)=\min_{a_0,a_1}\sum_{i=1}^{m}\left[B\left(\lambda_i,\hat{T}\right)\left(\hat{\varepsilon}_i\left(\hat{T}\right)-\left(a_0+a_1\lambda_i\right)\right)\right]^2 \tag{61}$$

Let us now consider the temperature $\hat{T}_{opt}$ for which the sum of square residues $R^2\left(\hat{T}\right)$ is minimum:

$$\hat{T}_{opt} = \arg\min_{\hat{T}}\left(R^2\left(\hat{T}\right)\right) \tag{62}$$

Remember that $\hat{\varepsilon}_i\left(\hat{T}\right)B\left(\lambda_i,\hat{T}\right) = S_i$, $i = 1,...,m$ for any value of $\hat{T}$ (see eq. (60)), in particular for $\hat{T}_{opt}$. Hence we have:

$$\hat{T}_{opt} = \arg\min_{\hat{T}}\left(\min_{a_0,a_1}\sum_{i=1}^{m}\left(S_i - (a_0 + a_1\lambda_i)B\left(\lambda_i,\hat{T}\right)\right)^2\right) \tag{63}$$

which shows that $\hat{T}_{opt}$ is also the temperature estimator obtained by the least-squares minimization involving a linear emissivity model.

Notice that the previous demonstration can be extended to a polynomial model of any degree. As a consequence, when dealing with a polynomial model of degree 0, the question changes to: *which distribution $\hat{\varepsilon}_i\left(\hat{T}\right)$ is closest to a horizontal line* ?

With a polynomial model of degree 2, it changes to: *which distribution $\hat{\varepsilon}_i\left(\hat{T}\right)$ is closest to a parabola* ?

The demonstration can actually be extended to any other analytical model for emissivity. In the end, the general question becomes: *which distribution $\hat{\varepsilon}_i\left(\hat{T}\right)$ is closest to the selected model* ?

We are actually far from the aim implicitly suggested by the regression methods proposed in the literature. As a matter of fact, the emissivity models (e.g. polynomial functions of the wavelength) used to perform a regression of the radiance signal, give the erroneous impression that the emissivity-profile solution we are looking for is a least squares approximation of the true emissivity profile (according to the chosen model). This is absolutely not the case, as demonstrated above and illustrated next.

In figure 6, the emissivity distribution $\hat{\varepsilon}_i\left(\hat{T}\right)$ corresponding to $\hat{T}$ =600K is the only one to be linear. The curvature of the profiles changes depending on whether $\hat{T}$ is higher or lower than 600K. If there is no error on the measured radiance, the best (actually perfect) match with a straight line is thus for $\hat{T}$ =600K, which is the right answer. Nevertheless, we has to admit that the profiles corresponding to an estimated temperature in the range 590K< $\hat{T}$ <610K are very close to a straight line. It is easy to imagine that with some experimental noise added, the square residuals obtained after the linear fit would be in the same range for all profiles $\hat{\varepsilon}_i\left(\hat{T}\right)$ corresponding to the former temperature range. A quantitative analysis of the noise influence will be given later.

The case in figure 7 is quite dramatic: it is evident that, among all possible solutions, the "true" profile is not the closest one to a straight line. Evidently, in this example, the distribution $\hat{\varepsilon}_i\left(\hat{T}\right)$ that is closest to a straight line is obtained for a temperature $\hat{T}_{opt}$ that is much higher than the "true" value of 600K (the profiles in the lower part of the figure are indeed smoother than those in the higher part). The final solution will thus present a bias. A bias would also be obtained for the case drawn in figure 7 if the chosen emissivity model was a polynomial of degree 0 instead of a polynomial of degree 1.

As often stated, when using LSMWP, it is necessary to choose an emissivity model that corresponds *exactly* to the true profile. The difficulty is that most often, the profile shape is unknown. A misleading thought is that LSMWP performs a fit of the true profile with the chosen model (polynomial, exponential, and so on). Actually, as seen above, performing LSMWP comes to choosing among the hypothetical solutions $\hat{\varepsilon}\left(\lambda,\hat{T}\right)$, the one which fits at best to the model, in the least squares sense by weighting it with the blackbody radiance (the fit deals with ε_i if the observable is radiance and with $\ln\left(\varepsilon_i\right)$ if it is the logarithm of radiance). This can lead to an emissivity profile of much higher or much lower mean value than the real one, together with an important temperature error. Actually, the problem with the classical LSMWP is that it sticks to the emissivity *shape* rather than to its *magnitude*.

5.2.4. Least squares solution of the non linear ETS problem

When using the Planck's law instead of the Wien's approximation, LSMWP cannot be linearized anymore. The nonlinear least squares problem can be tackled with the Levenberg-Marquardt method as provided for example by the *lsqnonlin* function from MATLAB library. When choosing a linear model for the emissivity and when the "true" emissivity profile is indeed linear this naturally leads to the right temperature and the right emissivity profile (there is no systematic error when the simulated emissivity spectrum corresponds to the chosen model). On the contrary, when the "true" emissivity profile is not linear, the identification presents a bias. For a "true" emissivity profile corresponding to the curve with circles in figure 7, the result is reported in figures 8 and 9. The circles in figure 8 correspond to the theoretical radiance (no noise is added at this stage) and the stars correspond to the spectral radiance calculated from $\hat{L}\left(\lambda_i,\hat{T}_{opt}\right)=\hat{\varepsilon}_{d1}(\lambda_i)B\left(\lambda_i,\hat{T}_{opt}\right)$ where $\hat{\varepsilon}_{d1}(\lambda)$ is the polynomial of degree 1 to which the distributions $\hat{\varepsilon}_i\left(\hat{T}\right)$ come closest (the one which is closest is $\hat{\varepsilon}_i\left(\hat{T}=652K\right)$. A perfect match for the radiance is of course impossible: the low order model chosen for emissivity (polynomial of degree 1) cannot explain the observed variations of the radiance.

The least squares procedure reveals that the $\hat{\varepsilon}_i\left(\hat{T}\right)$ distribution in figure 7 that fits at best to a straight line (taking into account the weighting with the blackbody radiance), is the one corresponding to the temperature $\hat{T}_{opt}$=652K. The stars in figure 9 correspond to $\hat{\varepsilon}_i\left(\hat{T}=652K\right)$ and the continuous curve is the unique line to which the distributions $\hat{\varepsilon}_i\left(\hat{T}\right)$ come at closest, namely $\hat{\varepsilon}_{d1}(\lambda)$. The systematic error is thus +52K for temperature and between -0.16 and -0.35 for emissivity.

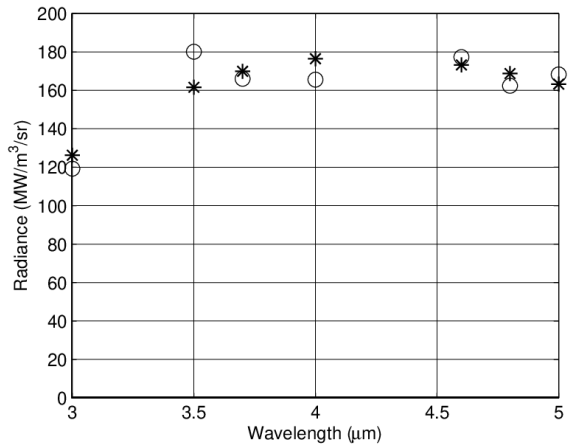

Figure 8. Inversion result for the emissivity profile represented with circles in figure 7 when using a linear model for emissivity. Here, the circles represent the "true" noiseless radiance (true temperature: T =600K), the stars correspond to the emitted radiance according to the solution (i.e. the emissivity distribution that is closest to a straight line, which is obtained for $\hat{T}_{opt}$ =652K)

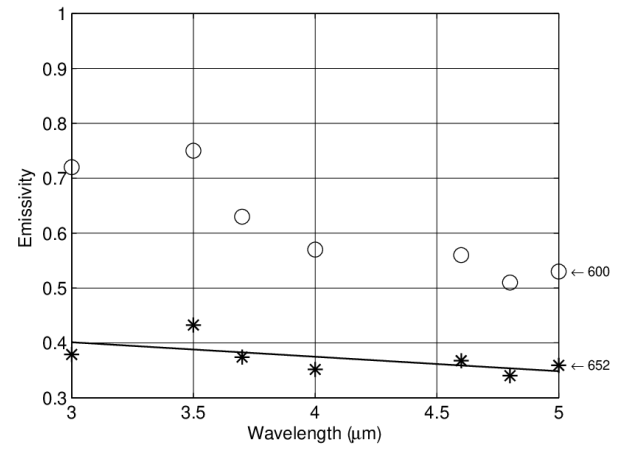

Figure 9. Inversion result for the emissivity distribution from figure 7 when using a linear model. The "true" emissivity distribution is shown with circles (T=600K). The solution is represented with stars (the associated temperature $\hat{T}_{opt}$ is 652K). The linear regression profile of the solution is represented with a continuous line ($\hat{\varepsilon}_{d1}(\lambda)$).

If the fitting happened be too far from the $\hat{\varepsilon}_i\left(\hat{T}_{opt}\right)$ profile, the model should be changed. For this particular example, however, changing to a quadratic model leads to a complete failure: the profile in figure 7 that is closest to a polynomial of degree 2 is the one corresponding to 500K and the retrieved (hypothetical) emissivity spectrum ranges between 1.4 and 3.7 ! Obviously the constraint $\hat{\varepsilon}_i\left(\hat{T}\right)$<1 should imposed. The acceptable solution would then be the profile associated to $\hat{T}$ =577K which nevertheless means a 23K underestimation.

Let us now analyze the influence of the measurement noise on the temperature and emissivity separation performance. This can be easily performed by simulating experiments where the theoretical radiance is corrupted with artificial noise. The radiance is altered by adding values that are randomly generated with a predetermined probability density function. We assumed a Gaussian distribution with a spectrally uniform standard deviation. We fixed it to a value ranging from 0.2% to 6% of the maximum radiance (additive noise). The least squares minimization was performed without constraint (i.e. without imposing ε_i<1) in order to highlight the mathematical (poor) stability of the inversion procedure. A series of 200 radiance spectra were treated for each noise level and for the two nominal emissivity profiles described in figures 6 and 7. We chose again a linear emissivity model for the LSMWP

inversion. The results for the maximum root mean square emissivity error among the seven channels are plotted in figure 10-left. Those for the root mean square error on temperature are plotted in figure 10-right. We can notice that:

- for the “true” profile of linear type (crosses), the RMS error on temperature and on emissivity increases proportionally to the radiance noise level. In particular, the RMS errors are 0.1 for emissivity and 12K for temperature when the noise is 1%.
- for the “true” profile of non-linear type (circles), the RMS errors are first dominated by the systematic error, which corresponds to the model implementation error (the chosen model –polynomial of degree 1 – is too crude to match the “true” profile); statistic errors due to the measurement noise dominate only when the noise is higher than 2-3%. The RMS errors are 0.36 for emissivity and 54K for temperature when the noise is 1%.

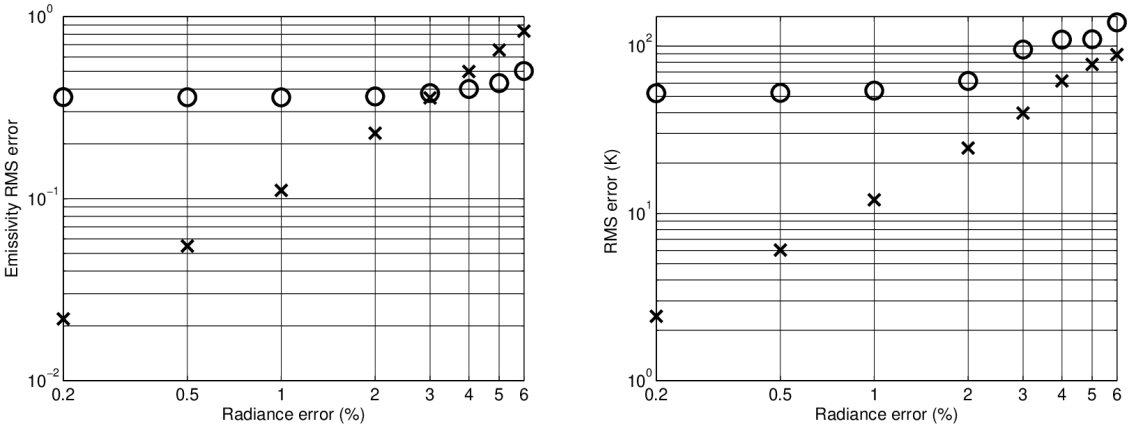

Figure 10. Statistic analysis (Monte Carlo sampling with 200 simulated experiments) of the measurement noise influence on the identified emissivity when using a linear emissivity model. The “true” emissivity was considered linear (crosses – refer to fig. 6) or non-linear (circles – refer to fig. 7). Multispectral measurement in seven channels between 3 and 5µm. Left : emissivity error, Right : temperature error.

Let us also add that the inversion leads to a systematic error as soon as the “true” profile departs from a straight line. The previous analysis allows us to evaluate the magnitude of this error when the deviation is small. Statistically, by considering several “true” profiles close to the nominal straight line in figure 6, the RMS of the systematic errors would be equal to the RMS of the statistic errors obtained by adding the same amount of measurement noise. For this reason, a “true” profile departing by as little as 1% from a straight line leads to an emissivity bias whose RMS value is about 0.1. The temperature quadratic mean error is in this case about 12K which is far from negligible. This result highlights the considerable importance of choosing the right emissivity model. This impact can be reduced by increasing the number of spectral channels (the trend is like $N^{-1/2}$), at the condition that the departure from the profile model is randomly distributed.

As a conclusion we can state that:

- Even by reducing the number of unknowns, as was done here by modeling the spectral emissivity with a polynomial of low degree, the problem remains badly conditioned; with a polynomial model (either for $\varepsilon(\lambda)$ or for $\ln\varepsilon(\lambda)$), reasonable inversion results are expected only when the degree is 1 or 0.
- Important systematic errors appear as soon as the real emissivity departs from the considered model: 1% departure from a straight line already leads to 12K RMS error. More complicated spectral shapes lead to unpredictably high systematic errors (54K for the considered example).
- Even if the real emissivity values at the sampled wavelengths *perfectly fitted* to a straight line, the demand on radiance measurement precision is very high: as a matter of fact no more than 0.2% noise is allowed to get a RMS error lower than 2.5K near 600K for a 7-band pyrometer between 3µm and 5µm.

Finally, LSMWP is not performing well for simultaneous evaluation of temperature and emissivity. Reasonable RMS values can be obtained only when the emissivity spectrum perfectly matches with the chosen emissivity model. Otherwise, important systematic errors are encountered. The problem is that, apart from a few exceptions, it is not known beforehand whether the emissivity of a tested material conforms to such a model or another.
The results are disappointing because the inversion is based on the emitted spectral radiance only. Good results can be obtained by taking advantage of the high spectral variability of accessory parameters like the atmosphere transmission and self-emission as well as the reflection of the environmental flux.

As a conclusion, it appears that there is no valuable reason to apply LSMWP in place of the simpler one-color or bispectral pyrometry. All methods need a priori information about the emissivity. However the requirements with one-color pyrometry (the knowledge of an emissivity level) or with bispectral pyrometry (the knowledge of the ratio of emissivity at two wavelengths) are less difficult to satisfy than the requirement with LSMWP which is *a requirement of a strict conformity of shape* of the emissivity profile with a given parametric function, which is practically impossible to satisfy.
Regarding LSMWP, it must finally be admitted that without knowledge of the *magnitude* of emissivity, the temperature measurement cannot be very precise. Some vague intuition about the shape of the emissivity spectrum is not sufficient and to add more wavelengths does not help much. The blackbody spectrum is extremely regular; therefore, the implementation of a polynomial model for the emissivity of degree greater than 1 introduces strong correlations and generally leads to poor results.

5.3. Another multiwavelength approach: the “TES” method

The “TES” method is a multiwavelength approach that was developed for land-surface temperature evaluation through infrared remote sensing, more specifically for the Advanced Space-borne Thermal Emission and Reflection Radiometer (ASTER) on board TERRA satellite [50]. It is a five-channel multispectral thermal–IR scanner.

TES is based on the observation that the relative spectrum $\beta(\lambda)=\hat{\varepsilon}(\lambda)/\bar{\hat{\varepsilon}}$ where the apparent emissivity $\hat{\varepsilon}(\lambda)$ is obtained from an estimation of temperature $\hat{T}$ according to:

$$\hat{\varepsilon}(\lambda,\hat{T})=\frac{L(\lambda,T)-L^{\downarrow}(\lambda)}{B(\lambda,\hat{T})-L^{\downarrow}(\lambda)} \tag{64}$$

is relatively insensitive to the temperature estimation error. A crude estimation as with the Normalized Emissivity Method (NEM) is thus sufficient [50]. The question is then how to extract the absolute spectrum $\hat{\varepsilon}(\lambda)$ from the relative spectrum $\beta(\lambda)$. Gillespie et al. [50] found out a correlation between $\varepsilon_{\min}$ and the minimum-maximum emissivity difference defined by $MMD=\beta_{\max}-\beta_{\min}$:

$$\varepsilon_{\min}\approx 0.994-0.687\,MMD^{0.737} \tag{65}$$

The regression was based on 86 laboratory reflectance spectra from the ASTER spectral library [11] for soils, rocks, vegetation, snow, and water between 10 and 14µm. Ninety five percent of the samples fall within 0.02 emissivity units of the regression line. Nevertheless, this empirical relation in not universal: data related to artificial materials like metals fall far below the regression line.

After evaluating $\varepsilon_{\min}$ from the regression law, we obtain a new estimate of the emissivity spectrum from:

$$\hat{\varepsilon}(\lambda)=\beta(\lambda)\frac{\varepsilon_{\min}}{\beta_{\min}} \tag{66}$$

The temperature $\hat{T}$ is finally obtained by inverting the Planck's law at a wavelength λ at which the emissivity profile $\hat{\varepsilon}(\lambda)$ reaches the highest value. One or two iterations are sufficient for the procedure to converge.

To be effective, TES requires at least three or four spectral bands. TES doesn't work well for near-grey materials (as a matter of fact $\varepsilon_{\min}$ would then stick to the value 0.994).

TES algorithm is presently used to calculate surface temperature and emissivity standard products for ASTER, which are predicted to be within respectively +1.5K and 0.015 of correct values. Validations performed on different sites demonstrated that TES generally performs within these limits.

The regression law:

$$\varepsilon_{\min}\approx 0.999-0.777\,MMD^{0.815} \tag{67}$$

was obtained using 108 emissivity spectra from the ASTER library, without man-made materials. It was compared with spectra of manmade materials used over urban surfaces in [57] (see fig. 11). The correlation in eq. (67) is relatively good for most considered manmade materials. Metallic surfaces are however badly modeled by this empirical relationship.

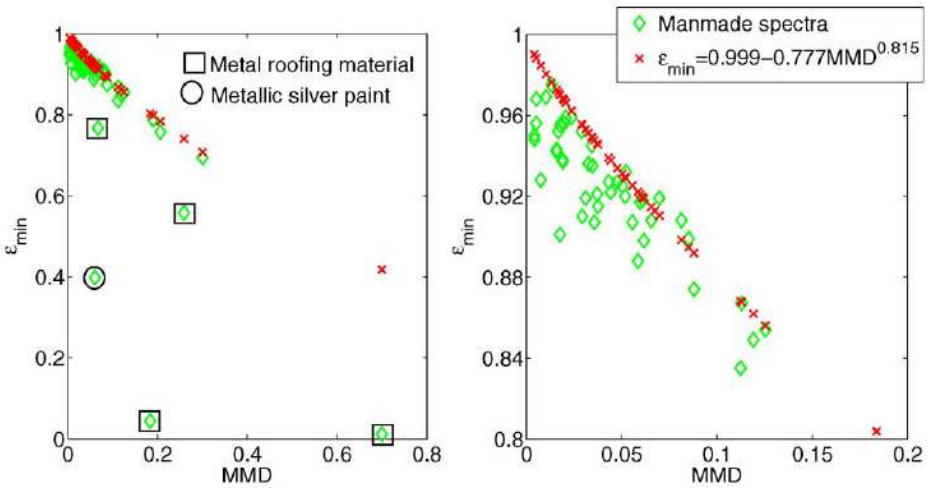

Figure 11. Correlation between MMD and $\varepsilon_{\min}$ in eq. (67) and comparison with 54 man-made materials spectra. Right figure is a detail from left plot [57].

The RMSE for emissivity is 0.017 in average (for a series of 9 manmade urban materials excluding metallic materials: brick, glass, tile, asphalt, concrete, marble, cement) and it may rise to 0.03 for some materials like marble and glass. Simultaneously, the RMSE for temperature is 0.9K in average and may rise to 1.5-1.8K for marble and glass ('true' temperature was set between 295K and 310K) [57].
The TES method is performing well for natural materials and man-made materials (excluding metallic materials) in the context of remote sensing. This concept could be extended to other situations. The decisive point would be to find out an empirical relation of the type shown in eq. (65) or (67) from the spectra of the considered materials.

5.4. The Bayesian approach for radiative thermometry

What has been exposed so far underlines the fact that a priori information on emissivity is is a prerequisite for the evaluation of temperature. Actually, the Bayesian framework allows taking into account any kind of a priori information on the parameters to estimate, hence it should be appropriate to solve the temperature-emissivity separation problem. However, although the application of Bayesian methods to thermal characterization is relatively common today [58], it is rather rare in multispectral pyrometry and multispectral/hyperspectral infrared remote sensing [59]-[65].
In the Bayesian framework the entire problem is modeled in terms of probability in order to allow for inference, that is, instead of attempting to obtain a single solution for the interesting unknowns it offers the possibility to explore the posterior distribution to determine the uncertainty in the unknowns given the measurements and *prior* uncertainty in the unknowns. The exploration calls for computing different point estimates like the maximum a posteriori estimate (MAP) and the conditional mean estimate (CM) as well as marginal distributions of individual unknowns or sets of unknowns [58], [66].
The parameters $\boldsymbol{\beta}$ (vector of size $(m+1)\times 1$) and the measurements $\mathbf{Y}$ (vector of size $m\times 1$) are considered as random variables. $\pi(\boldsymbol{\beta})$ is the *prior distribution* and it represents the uncertainty of the unknown prior to obtaining the measurement. The conditional distribution

of the measurements given the unknown is called the *likelihood distribution* and is denoted by $\pi(\mathbf{Y}|\boldsymbol{\beta})$. What interests us is the *posterior distribution* $\pi(\boldsymbol{\beta}|\mathbf{Y})$ which contains all information on the uncertainty of the unknowns $\boldsymbol{\beta}$ when the information on measurements $\mathbf{Y}$ is utilized [58], [66]. It is given by Bayes' theorem:

$$\pi(\boldsymbol{\beta}|\mathbf{Y}) = \frac{\pi(\mathbf{Y}|\boldsymbol{\beta})\pi(\boldsymbol{\beta})}{\pi(\mathbf{Y})} \tag{68}$$

where the denominator $\pi(\mathbf{Y})$ is obtained by marginalizing $\pi(\mathbf{Y}|\boldsymbol{\beta})$ over the parameters $\boldsymbol{\beta}$. It is merely a scaling constant; since it does not involve $\boldsymbol{\beta}$ it is generally discarded for most analyses:

$$\pi(\boldsymbol{\beta}|\mathbf{Y}) \propto \pi(\mathbf{Y}|\boldsymbol{\beta})\pi(\boldsymbol{\beta}) \tag{69}$$

Assume that the physical model is described by eq. (18) (negligible reflection effects) and that the measurement is corrupted by additive Gaussian noise with zero mean and covariance matrix $\boldsymbol{\Omega}$, which will be noted $\pi(\mathbf{e}) = N(0, \boldsymbol{\Omega})$ where $\mathbf{e}$ is the vector of the m spectral noise terms. The *likelihood distribution* $\pi(\mathbf{Y}|\boldsymbol{\beta}) = \pi(\mathbf{Y}|\boldsymbol{\varepsilon}, T)$ is then expressed by:

$$\pi(\mathbf{Y}|\boldsymbol{\varepsilon}, T) \propto \exp\left(-(\mathbf{Y} - \boldsymbol{\varepsilon} \otimes \mathbf{B})^T \boldsymbol{\Omega}^{-1} (\mathbf{Y} - \boldsymbol{\varepsilon} \otimes \mathbf{B})/2\right) \tag{70}$$

where $\boldsymbol{\varepsilon} = (\varepsilon_1 \ldots \ \varepsilon_m)^T$, $\mathbf{B} = (B(\lambda_1, T) \ldots \ B(\lambda_m, T))^T$ and $\otimes$ denotes the elementwise product.
On the other side, regarding the prior, we will assume that emissivity and temperature are independent variables, hence $\pi(\boldsymbol{\beta}) = \pi(\boldsymbol{\varepsilon})\pi(T)$. For ease, we will consider that the spectral emissivities are independent as well.

5.4.1. A simple example : single-color pyrometry

When there is only one spectral measurement, the *posterior distribution* $\pi(\boldsymbol{\beta}|\mathbf{Y})$ reduces to:

$$\pi(\varepsilon, T|Y) \propto \exp\left(-(Y - \varepsilon B(\lambda, T))^2 / 2\sigma^2\right)\pi(\varepsilon)\pi(T) \tag{71}$$

where σ is the noise RMS. If we are only interested in temperature, emissivity is then considered as a nuisance parameter. To obtain the posterior distribution for temperature alone, we thus have to marginalize the joint distribution $\pi(\varepsilon, T|Y)$ with respect to emissivity.
Let us consider for ease a uniform a priori distribution for emissivity: $\pi(\varepsilon) = U(\varepsilon_{\min}, \varepsilon_{\max})$.
The marginal posterior distribution related to temperature, $\pi(T|Y)$, can thus be expressed analytically [59]:

$$\pi(T|Y) \propto \frac{\pi(T)}{B(\lambda, T)}\left[\operatorname{erf}\left(\frac{Y - \varepsilon_{\max} B(\lambda, T)}{\sqrt{2}\sigma}\right) - \operatorname{erf}\left(\frac{Y - \varepsilon_{\min} B(\lambda, T)}{\sqrt{2}\sigma}\right)\right] \tag{72}$$

As an example, let us consider a monochromatic sensor at 4.7µm with 3% RMS noise, and assume that emissivity is expected to be in the range [0.5, 0.75]. If the measured radiance corresponds the radiance emitted by a surface at 600K with an emissivity of 0.6, the posterior distribution for temperature, given that measurement, is described by the black curve in fig. 11 (a non-informative prior has been considered for temperature, namely

$\pi(T) = U(500K, 700K)$). The curve is quite asymmetrical; the maximum a posteriori estimate is 582K whereas the conditional mean estimate is 597K, which is closer to the real value 600K. The distribution is quite large since the a priori distribution of the emissivity is large itself and the a priori distribution of temperature is non-informative. To shrink the a posteriori distribution we should have better information on the emissivity and possibly on temperature.

Let us now consider a measured radiance that is 8.3% higher than before. Among the infinite number of possibilities, it could correspond to the radiance emitted by a surface at 600K with an emissivity of 0.65. The posterior distribution for temperature is now given by the blue curve in fig. 11. The maximum a posteriori has risen to 592K and the conditional mean estimate to 606K. Let us pursue the analysis. If the measured radiance was 16.7% higher than the initial value (it could now correspond to the radiance emitted by a surface at 600K with an emissivity of 0.7), the posterior distribution for temperature is then given by the red curve. The maximum a posteriori has risen further to 600K and the conditional mean estimate to 615K.
Notice that for a progressively higher RMS noise, the curves would be progressively more rounded and approach a Gaussian curve.

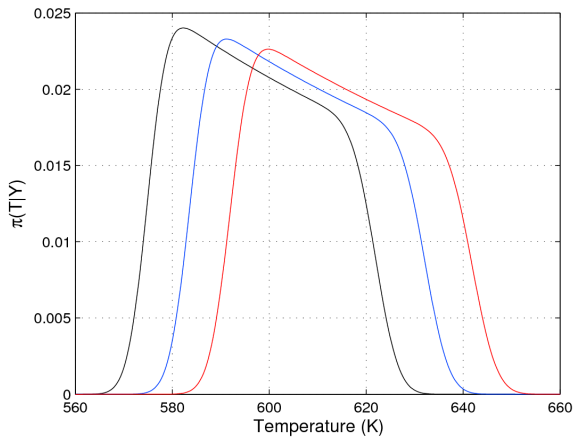

Figure 11. Posterior distribution of temperature in the case of uniform prior distribution of temperature and emissivity: $\pi(\varepsilon) = U(0.5, 0.75)$.
The measured radiance corresponds to the emitted radiance of a surface at 600K with an emissivity of 0.6 (black), 0.65 (blue) and 0.7 (red). Noise RMS is 3%.

As a final remark, let us say that thanks to the availability of a priori information on emissivity or temperature, the Bayesian approach allows to "anchor" the solution instead of providing an infinite set of equally acceptable solutions (ε, T). Nevertheless the "anchoring" is not bound to a particular solution set (ε, T), but rather loose. The poorer the a priori information, the more the "anchoring" is loose.

5.4.2. Multiwavelength pyrometry (linear approximation)

The implementation of the linear approximation for multiwavelength pyrometry (notably by introducing the Wien's law and considering the logarithm of the spectral signals S_i, $i = 1,...,m$ as the observables Y_i, $i = 1,...,m$, see eq. (35)) has the advantage, considering normal distributions for the priors and for the measurement noise, to yield analytical expressions.
Equation (35) can be rewritten as:

$$\mathbf{Y} = \mathbf{X}\boldsymbol{\beta} + \mathbf{e}' \tag{73}$$

where $\boldsymbol{\beta} = \left(\ln(\varepsilon_1) \ldots \ln(\varepsilon_m)\ T_{ref}/T\right)^T$ is the vector of (linear) parameters whose prior is a multivariate normal distribution of covariance matrix $\mathbf{W}$, namely $\pi(\boldsymbol{\beta}) = N\left(\boldsymbol{\beta}^{prior}, \mathbf{W}\right)$, whereas $\mathbf{e}'$ is the vector of additive errors with $\pi(\mathbf{e}') = N(0, \boldsymbol{\Omega})$ and $\mathbf{X}$ is the sensitivity matrix:

$$\mathbf{X} = \left(\mathbf{I}_{mm} \quad -\boldsymbol{\mu}_{m1}\right); \quad \boldsymbol{\mu} = \left(\mu_1\ \mu_2\ \ldots \mu_m\right)^T \tag{74}$$

where the constant coefficients μ_i, $i = 1,\ldots,m$ have been defined in eq. (36).
The posterior distribution $\pi(\boldsymbol{\beta}|\mathbf{Y})$ in eq. (69) becomes:

$$\pi(\boldsymbol{\beta}|\mathbf{Y}) \propto \exp\left(-\frac{1}{2}\left(\left(\mathbf{Y}-\mathbf{X}\boldsymbol{\beta}\right)^T \boldsymbol{\Omega}^{-1}\left(\mathbf{Y}-\mathbf{X}\boldsymbol{\beta}\right) + \left(\boldsymbol{\beta}-\boldsymbol{\beta}^{prior}\right)^T \mathbf{W}^{-1}\left(\boldsymbol{\beta}-\boldsymbol{\beta}^{prior}\right)\right)\right) \tag{75}$$

In the linear Gaussian case, all conditional distributions are Gaussian. It suffices therefore to compute the (conditional) means and covariances only (the maximum a posteriori estimator is equal to the (conditional) mean estimator) [66]. To obtain the maximum a posteriori estimator we differentiate the argument of the exponential in eq. (75) with respect to the parameter vector and look for the parameter vector that makes it vanish [66]. In the end we have:

$$\pi(\boldsymbol{\beta}|\mathbf{Y}) \propto \exp\left(-\frac{1}{2}\left(\left(\boldsymbol{\beta}-\hat{\boldsymbol{\beta}}_{MAP}\right)^T \Gamma_{\boldsymbol{\beta}|\mathbf{Y}}{}^{-1}\left(\boldsymbol{\beta}-\hat{\boldsymbol{\beta}}_{MAP}\right)\right)\right) \tag{76}$$

with the following expression for the maximum a posteriori estimator:

$$\hat{\boldsymbol{\beta}}_{MAP} = \Gamma_{\boldsymbol{\beta}|\mathbf{Y}}\left(\mathbf{X}^T\boldsymbol{\Omega}^{-1}\mathbf{Y} + \mathbf{W}^{-1}\boldsymbol{\beta}^{prior}\right) \tag{77}$$

where $\Gamma_{\boldsymbol{\beta}|\mathbf{Y}}$ is the posterior covariance matrix:

$$\Gamma_{\boldsymbol{\beta}|\mathbf{Y}} = \left(\mathbf{X}^T\boldsymbol{\Omega}^{-1}\mathbf{X} + \mathbf{W}^{-1}\right)^{-1} \tag{78}$$

Alternative expressions are [66]:

$$\hat{\boldsymbol{\beta}}_{MAP} = \boldsymbol{\beta}^{prior} + \mathbf{W}\mathbf{X}^T\left(\mathbf{X}\mathbf{W}\mathbf{X}^T + \boldsymbol{\Omega}\right)^{-1}\left(\mathbf{Y} - \mathbf{X}\boldsymbol{\beta}^{prior}\right) \tag{79}$$

and:

$$\Gamma_{\boldsymbol{\beta}|\mathbf{Y}} = \mathbf{W} - \mathbf{W}\mathbf{X}^T\left(\mathbf{X}\mathbf{W}\mathbf{X}^T + \boldsymbol{\Omega}\right)^{-1}\mathbf{X}\mathbf{W} \tag{80}$$

Notice that since $\mathbf{X}$ is full row rank rectangular matrix, and knowing that $\boldsymbol{\Omega}$ is positive definite, $\mathbf{X}^T\boldsymbol{\Omega}^{-1}\mathbf{X}$ is a singular (not invertible) matrix. However, adding the positive definite matrix $\mathbf{W}^{-1}$ makes the matrix $\left(\mathbf{X}^T\boldsymbol{\Omega}^{-1}\mathbf{X} + \mathbf{W}^{-1}\right)$ invertible. Hence, the *prior information* provides the *regularization* needed since $\mathbf{X}^T\boldsymbol{\Omega}^{-1}\mathbf{X}$ is singular. Beyond the presently underdetermined problem, it provides the regularization needed when $\mathbf{X}^T\boldsymbol{\Omega}^{-1}\mathbf{X}$ is ill-conditioned.

Equations (77) and (78) show that when the prior variance decreases while the measurement error variance is kept constant, the a priori solution progressively dominates the solution.

The following example intends to illustrate that multispectral measurements can lead to valuable results when combined to priors of good quality, at least for some of them.
The simplest case of bicolor pyrometry has been considered. The measurements are assumed to be performed at 3.7µm and 4.7µm with a noise RMS of 5%. The emissivity priors have mean values of 0.75 and 0.45 resp. at the first and second wavelength. In both cases the standard deviation is 0.1. On the other side, the temperature prior has a mean value of 650K and a quite large standard deviation, namely 150K in order to express that the temperature is not well known beforehand.
Consider now that the two measured spectral signals correspond to the radiances emitted by a surface at 600K with spectral emissivities of 0.7 and 0.5 (this will be referred as the set of "true" – unknown- values, which, we hope, the estimators will come close to). What are the MAP estimators and the uncertainty for temperature and emissivity? The application of the equations (77)-(80) provides the answer which is summarized in the following table:

Parameter	MAP estimator	stand. deviation
Temperature	598 K	11.7 K
emissivity at $3.7\ \mu\mathrm{m}$	0.72	0.09
emissivity at $4.7\ \mu\mathrm{m}$	0.51	0.05

The two next plots illustrate the marginal distributions for the three parameters (a priori and a posteriori). Notice that normal distributions apply to the transformed parameters $\left(\ln(\varepsilon_1)\ldots\ \ln(\varepsilon_m)\ \ T_{ref}/T\right)^T$; a backward transformation has been performed to plot the distributions of $\left(\varepsilon_1\ \ldots\ \varepsilon_m\ \ T\right)^T$.

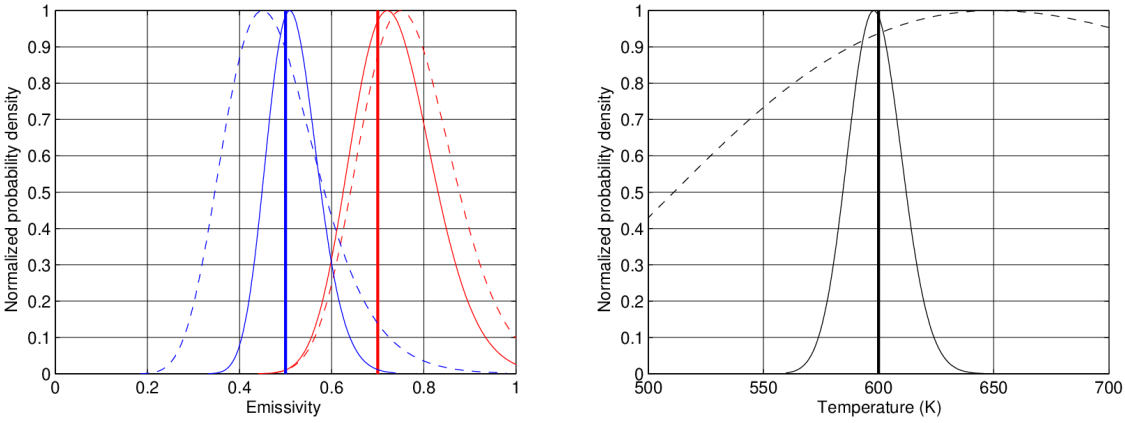

Figure 11. Left: normalized probability density of the emissivity at 3.7µm (in red) and at 4.7µm (in blue). The prior density is in dashed line, the posterior density is in continuous line. The "true" (unknown) values of the two emissivities (resp. 0.7 and 0.5) are indicated by vertical bold lines.
Right: normalized probability density of the temperature. The prior density is in dashed line, the posterior density is in continuous line. The "true" value of temperature (600K) is indicated by a vertical bold line.

Despite a temperature prior of poor quality, the estimators are quite close to the “true” values. Furthermore, if we compare the a priori distributions and the a posteriori distributions, we notice that the move was indeed towards the “true” values. In addition, the measurements contributed to shrink the distributions (all variances have decreased).
The simple analysis that has been performed so far can be extended to more than two wavelengths without any difficulty. The signals from multispectral or hyperspectral detectors can thus be processed and inverted directly (i.e. without iterations) through simple matrix algebra.

By the way, the former example clearly showed that a prior information on the magnitude of the spectral emissivities is of much higher value than a prior information that the emissivity profile belongs to a particular class of profiles (e.g. polynomial functions).

5.4.3. Multiwavelength radiometry (non-linear case)

The linear case developed in §5.4.2 presents a few limitations. One could argue that the Wien’s law is a mere approximation of the (exact) Planck’s law, however, as mentioned in §2.1, the approximation error is very small as long as the product λT is less than about 3000 µmK, which is the case when the spectral range is chosen in the rising part of the blackbody-radiance curve, namely where the sensitivity of the radiance to temperature is highest. The limitations come rather from the fact that in reality the emissivity and temperature priors are not necessarily Gaussians. As a matter of fact, some of the “theoretical” distributions in Fig. 11-left go beyond the boundary ε =1, which is unrealistic. For the emissivity, truncated prior distributions should thus be implemented. Moreover, we should be able to simulate probability distributions of arbitrary shape.
Beyond linear and Gaussian models, Bayesian inference requires a statistical estimation of the posterior probability distributions which involves numerical sampling. Markov chain Monte Carlo (MCMC) algorithms are implemented for obtaining a sequence of random samples from a probability distribution from which direct sampling is difficult. The Metropolis–Hastings algorithm [60] and the Gibbs’ sampler [62], [64], [65] are examples of MCMC algorithms.
The versatility of the MCMC algorithms makes them capable of handling radiative problems more complex than those described by the simple "pyrometric" equation in eq. (18). As such, the reflection contribution could be added in the unknown parameters since a good prior is generally accessible.
More details on MCMC algorithms can be found in the lecture devoted to Bayesian inference.

6. Conclusion

Accurate temperature measurement by radiative means is not an easy task. Many parameters have to be evaluated beforehand to extract the surface emitted radiance from the measured radiance (atmospheric contributions: self-emission and attenuation, reflections from the environment). We then face the problem of temperature-emissivity separation. This underdetermined problem requires that some knowledge about the emissivity of the tested material is introduced. The general feeling is that multiplying the spectral measurements at different wavelengths would help identify the temperature. The underdetermined nature of the problem is however invariably maintained. Introducing a model of the emissivity spectral

profile is often a misleading idea: high systematic errors inevitably occur when the model does not correspond perfectly to the real emissivity profile. Having some knowledge about the *magnitude* of emissivity is much more useful (but unfortunately more demanding) than imposing a particular class of *shapes*. The Bayesian framework is definitely well suited to this task.

7. References

[1] Siegel R and Howell J R 1972 *Thermal Radiation Heat Transfer* (McGraw Hill).

[2] Chrzanowski K and Szulim M 1998 Measure of the influence of detector noise on temperature measurement accuracy for multiband infrared systems *Applied Optics* **37**(22) 5051-5057

[3] Krapez J.-C. 2011 Radiative measurements of temperature in *Thermal Measurements and Inverse Techniques* (Taylor & Francis)

[4] Berk A., Conforti P., Kennett R., Perkins T., Hawes F., Van Den Bosch J. 2014 MODTRAN® 6: A major upgrade of the MODTRAN® radiative transfer code. *6th Workshop on Hyperspectral Image and Signal Processing: Evolution in Remote Sensing WHISPERS* pp. 1-4

[5] Labarre L., Caillault K., Fauqueux S., Malherbe C., Roblin A., Rosier B., Simoneau P. 2010 An overview of MATISSE-v2.0 *Optics in Atmospheric Propagation and Adaptive Systems XIII* SPIE Vol. 7828, p. 782802

[6] Loarer T., Greffet J.-J. and Huetz-Aubert, M. 1990 Noncontact surface temperature measurement by means of a modulated photothermal effect, *Appl. Optics* **29**(7) 979-987

[7] Loarer T., Greffet J.-J. 1992 Application of the pulsed photothermal effect to fast surface temperature measurements, *Appl. Optics* **31**(25) 5350-5358

[8] Amiel S., Loarer T., Pocheau C., Roche H., Aumeunier M. H., Gauthier E., LeNiliot C. and Rigollet, F. 2012 Surface temperature measurement of plasma facing components with active pyrometry. In Journal of Physics: Conference Series (Vol. 395, No. 1, p. 012074). IOP Publishing

[9] Amiel S., Loarer T., Pocheau C., Roche H., Gauthier E., Aumeunier M. H., Le Niliot C. Rigollet F., Courtois X., Jouve M., Balorin C. and V. Moncada V. 2014 2D surface temperature measurement of plasma facing components with modulated active pyrometry. *Rev. Sci. Instr.,* 85(10), 104905

[10] Touloukian Y S and DeWitt D P 1970 *Thermal radiative properties. Thermophysical properties of matter* (Plenum Corp. New-York)

[11] Salisbury J W and d'Aria D M 1992 Emissivity of terrestrial materials in the 8-14 µm atmospheric window *Remote Sens. Environ.* **42** 83-106

[12] Baldridge A M, Hook S J, Grove C I and Rivera G 2009 The ASTER Spectral Library Version 2.0 *Remote Sens. Environ.* **113** 711-715 http://speclib.jpl.nasa.gov/

[13] Corwin R R and Rodenburgh A 1994 Temperature error in radiation thermometry caused by emissivity and reflectance measurement error *Applied Optics* **33**(10) 1950-1957

[14] Hervé P and Sadou A 2008 Determination of the complex index of refractory metals at high temperatures: application to the determination of thermo-optical properties *Infrared Physics & Technology* **51** 249–255

[15] Pierre T, Rémy B and Degiovanni A 2008 Microscale temperature measurement by the multispecrtral and statistic method in the ultraviolet-visible wavelengths *J. Appl. Phys.* **103** 034904-1-10

[16] Duvaut T, Georgeault D and Beaudoin J L 1996 Pyromètre multispectral infrarouge : application aux métaux *Rev. Gen. Therm* **35** 185-196

[17] Hernandez D, Sans JL, Netchaieff A, Ridoux P, Le Sant V 2009 Experimental validation of a pyroreflectometric method to determine the true temperature on opaque surface without hampering reflections *Measurement* **42** 836-843

[18] Sentenac T., Gilblas R., Hernandez D., Le Maoult Y. 2012 Bi-color near infrared thermoreflectometry: A method for true temperature field measurement *Rev. Sci. Instr.* 83(12), 124902

[19] Sentenac T., Gilblas R., & Bugarin F. 2019 Trichromatic thermoreflectometry for an improved accuracy of true temperature field measurement on a multi-material part. *Int. J. Therm. Sci.* 145, 105980

[20] Krapez J-C, Bélanger C and Cielo P 1990 A double-wedge reflector for emissivity enhanced pyrometry *Meas. Sci. Technol* **1** 857-864

[21] Foley G.M. 1978 *High Temp. High Press*. **10**:391

[22] Watari M. Watanabe Y., Chigira S., Tamura Y., *Yokogawa Tech. Rep.* **29**:25

[23] Anderson 1985 *Adv. Instrument.* **40**:1337

[24] Tsai B.K., Shoemaker R.L., DeWitt D.P., Cowans B.A., Dardas Z., Delgass W.N., Dail G.J. 1990 Dual Wavelength radiation thermometry: emissivity compensation algorithms, *Int. J. Thermophysics* **11**(1) 269-281

[25] Gardner J L 1980 Computer modelling of a multiwavelength pyrometer for measuring true surface temperature *High Temp – High Press*. **12** 699-705

[26] Coates P B 1981 Multiwavelength pyrometry *Metrologia* **17** 103-109

[27] Gardner J L, Jones T P, Davies M R 1981 A six wavelength pyrometer, *High Temp – High Press*. **13** 459-466

[28] Hunter B, Allemand C D and Eager T W 1985 Multiwavelength pyrometry: an improved method *Opt. Eng.* **24**(6) 1081-1085

[29] Hunter B, Allemand C D and Eager T W 1986 Prototype device for multiwavelength pyrometry *Opt. Eng.* **25**(11) 1222-1231

[30] Hiernault J P, Beukers R, Heinz W, Selfslag R, Hoch M and Ohse R.W. 1986 Submillisecond six-wavelength pyrometer for high temperature measurements in the range 2000K-5000K *High Temp – High Press.* **18** 617-625

[31] Nordine P C 1986 The accuracy of multicolour optical pyrometry *High Temp. Sci.* **21** 97-109

[32] DeWitt D P and Rondeau R.E. 1989 Measurement of surface temperatures and spectral emissivities during laser irradiation *J. Thermophysics* **3**(2) 153-159

[33] Tank V and Dietl H 1990 Multispectral infrared pyrometer for temperature measurement with automatic correction of the influence of emissivity *Infrared Physics* **30**(4) 331-342

[34] Khan MA, Allemand C and Eager TW 1991 Noncontact temperature measurement. I. Interpolation based techniques *Rev. Sci. Instrum* **62**(2) 392-402

[35] Khan MA, Allemand C and Eager TW 1991 Noncontact temperature measurement. II. Least square based techniques Rev. Sci. Instrum **62**(2) 403-409

[36] Gathers G.R. 1991 Analysis of multiwavelength pyrometry using nonlinear least square fits and Monte Carlo methods *11th Symp. Thermophysic. Prop.* Boulder June 1991

[37] Lindermeir E, Tank V and Hashberger P 1992 Contactless measurement of the spectral emissivity and temperature of surfaces with a Fourier transform infrared spectrometer *Proc. SPIE* 1682 354-364

[38] Duvaut T, Georgeault D and Beaudoin JL 1995 Multiwavelength infrared pyrometry: optimization and computer simulations *Infrared Phys.& Technol*. **36** 1089-1103

[39] Chrzanowski K and Szulim M 1998 Error on temperature measurement with multiband infrared systems *Applied Optics* **38**(10) 1998-2006

[40] Chrzanowski K and Szulim M 1999 Comparison of temperature resolution of single-band, dual-band and multiband infrared systems *Applied Optics* **38**(13) 2820-2823

[41] Scharf V, Naftali N, Eyal O, Lipson S G and Katzir A 2001 Theoretical evaluation of a four-band fiber-optic radiometer *Appl Opt.* **40**(1) 104-111

[42] Mazikowski A and Chrzanowski K 2003 Non-contact multiband method for emissivity measurement *Infrared Phys. & Technol.* **44** 91-99

[43] Cassady L D and Choueiri E Y 2003 High Accuracy Multi-color Pyrometry for High Temperature Surfaces *IEPC-03-79 28th Int. Electric Propulsion Conference* Toulouse France March 17-21 2003

[44] Wen C D and Mudawar I 2004 Emissivity characteristics of roughened aluminium alloy surfaces and assessment of multispectral radiation thermometry (MRT) emissivity models *Int. J. Heat Mass Transfer* **47** 3591-3605

[45] Wen C D and Mudawar I 2004 Emissivity characteristics of polished aluminium alloy surfaces and assessment of multispectral radiation thermometry (MRT) emissivity models *Int. J. Heat Mass Transfer* **48** 1316-1329

[46] Sade S and Katzir A 2004 Multiband fiber optic radiometry for measuring the temperature and emissivity of gray bodies of low or high emissivity *Appl. Opt.* **43**(9) 1799-1810

[47] Uman I and Katzir A 2006 Fiber-optic multiband radiometer for online measurements of near room temperature and emissivity *Optic Letters* **31**(3) 326-328

[48] Duvaut T 2008 Comparison between multiwavelength infrared and visible pyrometry: application to metals *Infrared Phys.& Technol*. **51** 292-299

[49] Rodiet C., Remy B., Pierre T., & Degiovanni A. 2015 Influence of measurement noise and number of wavelengths on the temperature measurement of opaque surface with variable emissivity by a multi-spectral method based on the flux ratio in the infrared-ultraviolet range. *High Temp.--High Press.* **44**(3)

[50] Rodiet C., Remy B., & Degiovanni A. 2016 Optimal wavelengths obtained from laws analogous to the Wien's law for monospectral and bispectral methods, and general methodology for multispectral temperature measurements taking into account global transfer function including non-uniform emissivity of surfaces. *Infrared Phys.& Technol*. **76** 444-454

[51] Daniel K., Feng C., Gao, S. 2016 Application of multispectral radiation thermometry in temperature measurement of thermal barrier coated surfaces. *Measurement*, **92**, 218-223

[52] Zhang C., Gauthier E., Pocheau C., Balorin C., Pascal J. Y., Jouve M., Aumeunier M.H., Courtois X., Loarer T., Houry M. 2017 Surface temperature measurement of the plasma facing components with the multi-spectral infrared thermography diagnostics in tokamaks. *Infrared Phys.& Technol*. **81**, 215-222

[53] Bouvry B., Cheymol G., Ramiandrisoa L., Javaudin B., Gallou C., Maskrot H., Horny N., Duvaut T., Destouches C., Ferry L., Gonnier C. 2017 Multispectral pyrometry for surface temperature measurement of oxidized Zircaloy claddings. *Infrared Phys.& Technol*. **83**, 78-87

[54] Barducci A and Pippi I 1996 Temperature and emissivity retrieval from remotely sensed images using the “grey body emissivity” method *IEEE Trans. Geosci. & Remote Sensing* **34**(3) 681-695

[55] Gillespie A., Rokugawa S., Matsunaga T., Cothern J.S., Hook S., Kahle A.B. 1998 A temperature and emissivity separation algorithm for advanced spaceborne thermal emission and reflection radiometer (ASTER) images *IEEE Trans. Geosci. Remote Sens.* **36**(4): 1113-1126

[56] Sabol D.E., Gillespie A.R., Abbott E., Yamada G. 2009 Field validation of the ASTER temperature and emissivity separation algorithm *Remote Sens. Environ*. **113**: 2328-2344

[57] Oltra-Carrio R., Cubero-Castan M., Briottet X., Sobrino J. 2014 Analysis of the performance of the TES algorithm over urban areas *IEEE Trans. Geosci. Remote Sens.* **52**(11) 6989-6998

[58] Kaipio J. P., Fox C. 2011 The Bayesian framework for inverse problems in heat transfer *Heat Transf. Eng.* **32**(9), 718-753

[59] Morgan J. A. 2005 Bayesian estimation for land surface temperature retrieval: The nuisance of emissivities. *IEEE Trans. Geosci. Remote Sens***. 43**(6) 1279-1288

[60] Heasler P., Posse C., Hylden J., Anderson K. 2007 Nonlinear bayesian algorithms for gas plume detection and estimation from hyper-spectral thermal image data. *Sensors*, **7**(6), 905-920

[61] Morgan J. A. 2011 Comparison of Bayesian land surface temperature algorithm performance with Terra MODIS observations *Int. J. Remote Sens.* **32**(23) 8139-8159

[62] Berrett C., Williams G. P., Moon T., & Gunther J. 2014 A Bayesian Nonparametric Model for Temperature-Emissivity Separation of Long-Wave Hyperspectral Images *Technometrics* **56**(2) 200-211

[63] Krapez J.-C. 2015 Measurements without contact in heat transfer: principles, implementation and pitfalls *METTI 6* Advanced School:Thermal Measurements and Inverse Techniques, Biarritz, March 1- 5, 2015

[64] Ash J. N., Meola J. 2016 Temperature-emissivity separation for LWIR sensing using MCMC. *Algorithms and Technologies for Multispectral, Hyperspectral, and Ultraspectral Imagery XXII SPIE* Vol. 9840, p. 98401O

[65] Toullier T., Dumoulin J., & Mevel L. 2018 Etude de sensibilité de différentes méthodes de séparation pour l'évaluation simultanée de l'émissivité et de la température par thermographie infrarouge multispectrale, Congrès SFT, Pau.

[66] Kaipio J., Somersalo E. 2006 *Statistical and computational inverse problems* (Vol. 160). Springer Science & Business Media.